Targeting of the nuclear RNA exosome to chromatin by HP1 affects the transcriptional program of liver cells.

Hiba SOUAIFAN 1,4, Mickael COSTALLAT 1, Laura SITKIEWICZ 2, Kylian GODEST 3, Florence CAMMAS 2, Carl MANN 3, Christian MUCHARDT 1*, Christophe RACHEZ 1*

1. Institut de Biologie Paris-Seine (IBPS), Sorbonne Université, CNRS UMR7238, 75252 Paris, France
2. Institute of Human Genetics, CNRS UMR9002 University of Montpellier, 34396 Montpellier, France
3. Institut de Biologie Intégrative de la Cellule (I2BC), CEA, CNRS, Université Paris-Saclay, 91190 Gif-sur-Yvette, France
4. Ecole doctorale Complexité du Vivant, Sorbonne Université, Paris, France
* Co-corresponding authors.

Abstract

RNA maturation and degradation processes occurring co-transcriptionally are modulated by the structure of chromatin and they are influenced by chromatin-associated factors such as HP1. Beyond their classical definition as markers of the pericentromeric heterochromatin, the three mammalian HP1 proteins have been requalified as regulators of several co-transcriptional processes occurring on chromatin such as alternative splicing. We uncover here a novel association of HP1 with the nuclear RNA exosome, a complex involved in RNA degradation. Mouse embryonic liver-derived cells depleted in all three HP1 proteins displayed increased levels of various RNA species genome-wide, showing stabilization of transcripts from retrotransposon-like repeated elements and stabilization of certain gene- and enhancer-associated transcripts. Our results demonstrate that the RNA exosome interacts with HP1 proteins and is targeted to chromatin loci through HP1-dependent mechanisms, leading to the degradation of unstable chromatin-associated transcripts. Detection of such transcripts in the absence of HP1 was correlated with a gain in chromatin accessibility, as defined by ATAC-seq. The consequent increased activity of nearby genomic elements corresponding to poised liver enhancers resulted in an upregulation of genes expressing extracellular matrix components such as *Col6a1* and *Col6a2*. In our re-analysis of a previous hepatocellular carcinoma study, patients with the highest levels of inflammation showed reduced HP1 levels and less RNA degradation. This reduction leads to tumors with unique characteristics linked to collagen gene upregulation, being potentially more rigid and exhibiting lower proliferation. These findings illustrate the role of HP1 proteins in regulating RNA homeostasis through their interaction with the RNA exosome, suggesting important implications for cancer biology.

Introduction

Chromatin structure is a major regulator of transcription. This regulation is mediated by molecular machineries that establish transcriptionally active or repressed chromatin states, known as euchromatin and heterochromatin, respectively. In active regions, chromatin influences gene expression programs that govern processes ranging from development to responses to external stimuli. In contrast, constitutive heterochromatin is typically found at pericentromeric regions and transposable elements, and is enriched with repressive epigenetic marks— notably di- and tri-methylation of histone H3 on lysine 9 (H3K9me2/3). These marks serve as binding sites for HP1 proteins, which are essential for the establishment, maintenance, and propagation of heterochromatin (for a review,(Grewal, 2023).

The three mammalian HP1 isoforms—HP1α, HP1β, and HP1γ—share a conserved structure consisting of two globular domains separated by an intrinsically disordered hinge region. The N-terminal chromodomain specifically recognizes and binds H3K9me2/3-marked nucleosomes, anchoring HP1 to heterochromatic regions (Bannister *et al*, 2001; Jacobs *et al*, 2001; Lachner *et al*, 2001). The C-terminal chromoshadow domain mediates dimerization and interactions with a broad range of PxVxL motif–containing proteins involved in transcriptional regulation, DNA replication, and repair (Lechner *et al*, 2005; Thiru *et al*, 2004). The unstructured hinge region has an affinity for nucleic acids (for review: (Hiragami-Hamada & Fischle, 2014). In addition to their well-established role in heterochromatin, HP1 proteins also localize to actively transcribed genes in both *Drosophila* and mammals, with isoform-specific patterns (Minc *et al*, 2000; Piacentini *et al*, 2009; Vakoc *et al*, 2005). In euchromatin, HP1 proteins have been implicated in several co-transcriptional processes, including the regulation of alternative splicing (Allo *et al*, 2009; Ameyar-Zazoua *et al*, 2012; Saint-Andre *et al*, 2011; Smallwood *et al*, 2012; Yearim *et al*, 2015), recruitment of RNAi machinery to chromatin (Ameyar-Zazoua *et al*, 2012), and control of transcriptional elongation (Porozhan *et al*, 2024) and termination (Skourti-Stathaki *et al*, 2014).

Multiple lines of evidence indicate that the RNA-binding activity of HP1 proteins underlies their functions in both euchromatin and heterochromatin. In both compartments, HP1 proteins engage with repeated RNA sequences. This was first demonstrated by the requirement of RNA binding for HP1 targeting to heterochromatin (Maison *et al*, 2002; Muchardt *et al*, 2002). Later, it was further shown that HP1α specifically associates with pericentromeric major satellite repeat RNA (SatRNA) (Maison *et al*, 2011). More recently, we showed that HP1γ contributes to splicing precision by recognizing hexameric motifs enriched in intronic SINE elements, supporting intron–exon discrimination and contributing to accurate splice site definition (Mata-Garrido *et al*, 2022; Rachez *et al*, 2021). In *Schizosaccharomyces pombe*, recognition of repeated sequences by the HP1 homolog Swi6 has been further linked to the degradation of satellite RNAs (SatRNAs), contributing to transcriptional repression beyond chromatin condensation. Two distinct mechanisms may mediate this repression. First, Swi6 is required for RNAi-dependent silencing by directing SatRNA to the RITS complex, enabling siRNA production via double-stranded RNA formation (Motamedi *et al*, 2008). Second, silencing at centromeric repeats and the silent mating-type locus—both heterochromatic regions—also involves polyadenylation-dependent RNA degradation via the RNA exosome cofactor Cid14 (Buhler *et al*, 2007). Swi6 then engages in a

dynamic exchange between free, chromatin-bound, and RNA-bound states, facilitating the delivery of repeat-derived RNAs to degradation machineries (Keller *et al*, 2012).

The RNA exosome complex is a central machinery for RNA degradation and quality control in eukaryotic cells (Kilchert *et al*, 2016). Its core structure consists of nine non-catalytic subunits (Exosc1–9) that form a scaffold for associated 3′→5′ ribonucleases. In the cytoplasm, the exosome partners with the ribonuclease Dis3l and cytoplasmic cofactors to form the SKI complex, which mediates mRNA turnover and surveillance (Tomecki *et al*, 2023). In the nucleus, the exosome associates with two ribonucleases: Rrp6/Exosc10, a distributive exonuclease, and Rrp44/Dis3, a processive exo- and endonuclease. The nuclear exosome functions within specialized complexes—NEXT, PAXT, and TRAMP—that provide substrate specificity across a broad spectrum of nuclear RNAs (Rambout & Maquat, 2024). The TRAMP complex, well characterized in *S. cerevisiae*, contributes to ribosomal RNA processing and snoRNA precursor degradation. In mammals, however, TRAMP is primarily restricted to the nucleolus (LaCava *et al*, 2005). By contrast, the NEXT complex targets unprocessed RNAs with a free 3′ end, such as promoter-upstream transcripts (PROMPTs), uaRNAs, and enhancer RNAs (eRNAs) (Andersson *et al*, 2014; Lubas *et al*, 2011; Preker *et al*, 2008), while the PAXT complex directs degradation of polyadenylated nuclear RNAs (Meola *et al*, 2016). A defining feature of all exosome complexes is the presence of an RNA helicase. In the cytoplasm, this activity is provided by Ski2, while in the nucleus, Mtr4 is essential for substrate recruitment to NEXT, PAXT, and TRAMP (reviewed in (Weick & Lima, 2021). Recruitment of these nuclear complexes is further mediated by the cap-binding complex (CBC), which recognizes the 5′ methyl-guanosine cap of RNA polymerase II transcripts. CBC, along with its cofactor ARS2, connects to NEXT via the zinc-finger protein ZC3H18, forming the CBC–NEXT axis (Andersen *et al*, 2013). ZC3H18 bridges the 5′ cap to the exosome, facilitating the degradation of unstable or aberrant RNAs.

The activity of the RNA exosome has previously been linked to the organization of chromatin structure. At a large scale, chromatin architecture, particularly topologically associating domains (TADs) and chromatin loops, is shaped by architectural proteins such as CTCF and cohesins (Phillips & Corces, 2009). Depletion of the nuclear exosome subunit DIS3 impairs non-coding RNA processing, reduces CTCF binding, and disrupts TAD organization at the *Igh* locus (Laffleur *et al*, 2021). In parallel, transcripts derived from normally silenced retroelements are targeted for degradation by the NEXT complex, which recognizes unstable RNAs arising from heterochromatic regions (Garland *et al*, 2022; Wu *et al*, 2019). Mass spectrometry (MS) approaches have finally suggested that RNA exosome-associated factors such as ZC3H18 and the RNA helicase MTR4 may associate with HP1 (Silla *et al*, 2020; Winczura *et al*, 2018), while, reciprocally, HP1 MS data has detected ZC3H18 among the interacting partners of all three HP1 isoforms (Zaidan *et al*, 2018). This association suggest that molecular bridges may exist between chromatin, HP1, and nuclear RNA degradation machineries.

Building on this possible connection, we have here analyzed the relationship between chromatin-associated HP1 proteins and RNA exosome components in murine BMEL liver cell lines depleted of all three HP1 isoforms. Previous studies using these cells showed that HP1 depletion results in the accumulation of transcripts from normally silenced retroelements, including LINEs, SINEs, and LTR-containing endogenous retroviruses (ERVs) (Calvet *et al*, 2022; Saksouk *et al*, 2020). In this context, we confirm physical associations between HP1 proteins

and several representative components of the nuclear exosome, and show an HP1-dependent enrichment of exosome complexes at chromatin loci. HP1 loss also led to a marked increase in chromatin-associated unstable transcripts, such as PROMPTs and retroelement-derived RNAs, particularly at LTR loci. Notably, some of these transcripts extended beyond the annotated repeat boundaries and were detected in a mature form in the cytoplasm. In parallel, enhancers located near these retroelements became activated in the absence of HP1, leading to upregulation of adjacent genes and widespread alterations in transcriptional programs.

Results

HP1 proteins interact with components of the RNA Exosome and affect their subcellular localization.

Analysis of ZC3H18 immunoprecipitation–mass spectrometry data (Winczura *et al*, 2018) using the STRING database (Search Tool for the Retrieval of Interacting Genes/Proteins) documented that the protein-protein interactions linking the RNA exosome and the Cap binding complex with the three HP1 proteins and other epigenetic regulators, were supported by multiple independent sources (Fig. 1A, each "string" represents a documented protein-protein interaction). This prompted us to further investigate the links between HP1 proteins and the nuclear RNA Exosome.

To this end, we compared mouse embryonic liver (BMEL) cells lacking all three HP1 isoforms (triple knockout, TKO) to HP1-expressing controls (Het, heterozygous for HP1α and wild type for HP1β and HP1γ). Six independent clones were analyzed: TKO1, TKO2, TKO3, and Het1, Het32, Het35 (Fig. 1B and Supplemental Fig.1A). Western blot analysis of total extracts showed that protein levels of EXOSC3 and EXOSC9 (core exosome subunits), MTR4 (a nuclear RNA helicase common to all nuclear exosome complexes), and ZC3H18 (a zinc-finger adaptor protein specific to the NEXT complex) were similar between Het and TKO clones, indicating that HP1 depletion did not affect their overall expression (see representative clones, Fig. 1C). Upon fractionation of the Het clones into cytosolic (C), nucleosolic (N), and chromatin (X) extracts, the four proteins were predominantly detected in the nucleosolic and chromatin fractions, which were also enriched in HP1γ (Fig. 1D). Interestingly, in the TKO clones, we observed increased accumulation of EXOSC9 and EXOSC3 in the cytosolic fraction, suggesting reduced nuclear retention of these subunits (Fig. 1D, lanes C). Fractionation quality was validated by Western blotting for marker proteins and by analyzing the distribution of representative cytoplasmic and nuclear transcripts (Supp. Fig. 1A–C).

Finally, co-immunoprecipitation from nuclear extracts containing both soluble and chromatin-associated material confirmed an association of HP1 proteins with EXOSC9, EXOSC10, MTR4, and ZC3H18, consistent with the previously reported MS data (Fig. 1E-G and Supp. Fig. 1D-E). These interactions were maintained following RNase treatment (Supp. Fig. 1F), indicating that they were not mediated by RNA. Together, these results further documented interactions between the HP1 proteins and components of the RNA exosome machinery, and suggested that these interactions are required for full nuclear retention of certain exosome subunits.

Several non-coding, unstable RNA species are found stabilized in the absence of HP1 proteins, in both chromatin and cytosolic fractions.

We next used RNA-seq to examine RNA profiles in chromatin and cytosolic fractions of the BMEL Het and TKO clones (Fig. 1B). In this setup, the chromatin fraction was expected to be enriched in nascent and incompletely processed RNAs, whereas the cytosolic fraction was expected to be depleted of unstable nuclear transcripts and enriched in mature mRNAs (Supp. Fig. 1C). In parallel, RNA-seq was also performed on total RNA from each clone.

The RNA species we examined included various RNAs encoded by LTRs, LINEs, SINEs, and MMSAT repeats. For these, we focused on extragenic repeat elements, excluding those located within gene bodies, such as intronic repeats, which may be transcribed incidentally as part of coding gene expression and processed in that context. We also examined levels of upstream antisense uaRNA at promoters (PROMPT RNA), and eRNA at active distal enhancers (enhD RNA), all documented as unstable transcripts. Genomic elements were considered as expressed when yielding at least two RNA-seq reads in at least one experimental condition.

Using this criterion, levels of unstable transcripts increased in TKO cells compared to HP1-expressing (Het) cells. In particular, we noted that for more than 50% of all expressed LTR elements, expression was detected exclusively in TKO cells (see examples in Fig. 2A, and quantification in Fig. 2B). Several elements were also expressed exclusively in Het cells, reflecting the multiplicity of HP1 functions not solely linked to RNA stability (Hediger & Gasser, 2006). Global analysis of RNA abundance further showed that mean RNA levels from PROMPTs, distal enhancers (enhD), and repeat elements (LTRs, LINEs, SINEs) were increased in the chromatin fraction of TKO cells relative to Het (Fig. 2C). In contrast, chromatin-associated pre-mRNAs from Ensembl-annotated genes, measured by exonic reads, were less affected by HP1 depletion. Globally, the Ensembl gene transcript category showed more moderate changes in both RNA levels and the number of loci with TKO- or Het-specific expression compared to non-coding RNA categories (Fig. 2E-G). These findings suggest that HP1 loss predominantly affects the expression and/or stability of unstable, non-coding RNAs, rather than processed mRNAs. Supporting this, several non-coding RNAs that accumulated in the chromatin fraction—particularly those derived from LTRs, LINEs, and MMSAT repeats—were also found at higher levels in the cytoplasm of TKO cells (Fig. 2D). In addition, many LTR-initiated transcripts extended for several kilobases and, interestingly, some appeared to be spliced in the cytoplasm (e.g., RLTR17, RMER13A; Fig. 2A), suggesting that in the absence of HP1, these RNAs evade nuclear decay and undergo canonical maturation.

Notably, several of the LTR-derived transcripts most readily detected in TKO cells (Fig. 2H, green and red profiles) were also reported as overexpressed in a previous study following depletion of ZFC3H1 or ZCCHC8, components of the PAXT and NEXT nuclear exosome pathways, respectively, in mouse embryonic stem cells (Garland *et al*, 2022); Fig. 2H, yellow and light blue profiles). While derived from a different cell type, this overlap supports the idea that the accumulation of LTR transcripts observed in TKO cells reflects impaired exosome-mediated RNA degradation. Together, these results suggest that HP1 loss stabilizes normally unstable non-coding RNAs, possibly due to defective degradation at the chromatin level.

An HP1-dependent association of nuclear RNA exosome and cofactors to chromatin loci.

Having observed that HP1 inactivation alters the nuclear retention of RNA exosome components and leads to the accumulation of unstable RNAs on chromatin, we next sought to examine more closely how RNA exosome components associate with nuclear structures. We therefore performed chromatin immunoprecipitation followed by high-throughput sequencing (ChIP-seq) with anti-EXOSC10, -ZC3H18, and -MTR4 antibodies using the Het32 and the TKO2 clones. To also gain insight in the overall impact of HP1 inactivation on chromatin structure, we completed this series of experiments with anti-CTCF, and anti-phospho RNA polymerase II (P-

RNAPII, as a mix of both phospho-Ser2 and -Ser5 forms) ChIP-seq, and HP1α, HP1β, HP1γ, H3K9me3, and H3K27me3 CUT&Tag experiments (Fig. 3A).

Examination of the ChIP-seq profiles with a genome browser revealed that the nuclear exosome components, MTR4, ZC3H18, and EXOSC10 are actively recruited to chromatin at specific genomic loci. This recruitment was most clearly detected in regions also recruiting P-RNAPII, while Mtr4 also displayed an interesting overlap with CTCF. Importantly, the chromatin recruitment of exosome components was strongly diminished in TKO2 cells, indicating that HP1 proteins are required for their proper localization to these regions. In contrast, levels of phosphorylated RNA polymerase II (P-RNAPII) appeared increased in TKO2 cells (Fig. 3A). Quantification of MTR4, ZC3H18, and EXOSC10 ChIP-seq peaks detected with the MACS2 package confirmed a dramatic decrease in the number and/or intensity of these peaks upon inactivation of the HP1 genes, while the total number of P-RNAPII peaks was strongly increased (Fig. 3B-C).

Metagene analysis on more than twenty thousand genes confirmed a preferential enrichment of MTR4, ZC3H18, EXOSC10 on the body of genes, with a peak at the transcription start site (TSS - Fig. 3D). Thus, the distribution of these factors coincided with that of the P-RNAPII, although missing accumulation at sites of transcription termination (TES). This analysis further revealed that HP1 inactivation led to a uniform reduction in RNA exosome component-occupancy over gene bodies, while RNAPII occupancy was correspondingly increased (Fig. 3D, compare brown and dark blue profiles). CUT&Tag analysis of the recruitment of each HP1 isoform in Het cells showed their preferential enrichment at gene transcriptional start sites (TSS, blue profiles Fig. 3E), compared to the background HP1 alpha CUT&Tag signal in TKO cells (orange profile Fig. 3E). This distribution of HP1 proteins at actively transcribed genes is consistent with earlier reports (Ostapcuk *et al*, 2018). It is also compatible with a co-recruitment of HP1 and RNA exosome proteins at promoter regions. Thus, HP1 inactivation leads to both reduced recruitment of the RNA degradation machinery and increased recruitment of RNA polymerase II, supporting a model in which HP1 proteins contribute to gene silencing by simultaneously restricting transcription and promoting RNA degradation. Of note, although HP1 enrichment at TSS was not associated with H3K9me3 or H3K27me3 marks, HP1 colocalized with H3K9me3 at other regions, such as simple repeats (Fig. 3E and 3F, and Supp. Fig. 3A and 3B). At these sites, HP1 inactivation did not lead to a loss of H3K9me3 but rather to a redistribution of the mark across repeats. These observations suggest that the targeting of the RNA exosome to TSS by HP1 and its association with H3K9me3 at other loci rely on two independent mechanisms.

HP1 concentrates MTR4 and CTCF at gene promoters.

We next examined in more detail the apparent colocalization of MTR4 with CTCF peaks. Quantification confirmed that 90% of the MTR4 peaks match CTCF peaks (representing approximately 15% of the total number of CTCF peaks). It also showed that MTR4 was the only RNA exosome component under scrutiny to display this colocalization (Fig. 4A). Comparison of ChIP-seq data between Het32 and TKO2 cells showed that the overall number of CTCF peaks remained broadly unchanged following HP1 depletion (Fig. 4B). However, genome browser visualization revealed a redistribution of CTCF binding: in TKO2 cells, new CTCF peaks appeared at previously annotated loci where no binding was detected in Het32 cells, while many pre-existing

peaks decreased in intensity, eventually below levels of detection (Fig. 4C). Heatmap analyses confirmed this genome-wide redistribution of CTCF occupancy (Fig. 4D). The genome-browser visualization further suggested that a large fraction of the CTCF peaks colocalizing with MTR4 were located at promoters. Sorting promoters according to HP1 occupancy revealed that CTCF and MTR4 were co-enriched at HP1-bound promoters in Het32 cells and that HP1 inactivation led to a strong reduction of both CTCF and MTR4 enrichment at these sites, accompanied by an increase in P-RNAPII signal (Fig. 4E). Together, these results suggest that HP1 proteins contribute to concentrating both CTCF and MTR4 at a subset of promoters, possibly also preventing it from ectopic associating with other CTCF binding sites.

A gain in chromatin accessibility at enhancers affects collagen gene expression

To gain broader insight into the regulatory elements impacted by HP1 inactivation, we intersected both CTCF ChIP-seq peaks and HP1 CUT&Tag peaks with the catalog of candidate cis-regulatory elements (cCREs) annotated by the ENCODE project (Supp. Fig. 5A and Fig. 5A). This analysis revealed that CTCF peaks were located within annotated regulatory elements, including promoters and enhancers, both locations where they were mostly lost in the absence of HP1 (Supp. Fig. 5A). In parallel, approximately 40% of HP1 peaks were also located within promoters as well as enhancers, with a predominance of distal (enhD) versus promoter-proximal enhancers (enhP) (Fig. 5A). To further investigate the consequences of HP1 loss on enhancer activity in BMEL cells, we performed ATAC-seq in Het and TKO clones. Based on chromatin accessibility profiles, distal enhancers (enhD) were categorized as active in both conditions, with decreased activity in TKO cells, with increased activity in TKO cells, or inactive (Unchanged, Down, Up, Inactive, respectively. Supp. Fig. 5B). Heatmap analyses revealed that, similar to observations at promoters, a substantial fraction of active enhancers were associated with HP1 in Het cells (Fig. 5B).

Importantly, activation of enhancers upon HP1 inactivation correlated with the upregulation of nearby genes located within 100 kb (enhD Up, orange bar, Fig. 5C). Gene ontology analysis of these upregulated genes revealed a strong enrichment for terms associated with the collagen-containing extracellular matrix (Fig. 5D). Further examination showed that multiple collagen isoforms were specifically upregulated at enhancers derepressed upon HP1 inactivation, as exemplified at the Col6 locus (Fig. 5E, and list in Supp. Fig. 5C). This activation correlated with an increased accumulation of transcripts over the enhD elements in the chromatin fraction, and at some loci, also in the cytosolic fraction, suggesting increased stability of enhancer RNAs (eRNAs)—potentially a consequence of the reduced recruitment of RNA exosome components to chromatin (Fig. 5E, arrows; Sup. Fig. 5B). This mechanism may also be at play for the few thousand LTR retroelement transcripts that were stabilized in TKO (Sup. Fig. 5D). These findings suggest that collagen genes are particularly sensitive to decreased RNA exosome activity. To further support this hypothesis, we analyzed publicly available transcriptomic datasets from Exosc3 conditional knockout mouse embryonic stem cells (GSE100535, Fig. 5F) and HeLa cells depleted of ZFC3H1 (GSE212557, Fig. 5G). Remarkably, in both models, genes associated with the collagen-containing extracellular matrix were among the most significantly affected pathways following disruption of RNA exosome activity.

HP1 Deficiency and Reduced RNA Exosome Activity Converge to Deregulate Collagen Genes in Hepatocellular Carcinoma

To investigate the relevance of the cooperation between HP1 proteins and the RNA exosome in hepatocellular carcinoma (HCC), we reanalyzed RNA sequencing data from a cohort of 76 Mongolian HCC patients (Candia *et al*, 2020). The molecular subtypes identified in this cohort largely mirrored those previously described in patients from other geographic regions, including Asia, Europe, and North America. Our analysis revealed that HP1 gene expression—including CBX3, CBX1, and CBX5—was upregulated in the majority of tumors, with 71% of cases showing at least a twofold increase relative to adjacent healthy tissues (Supp. Fig. 6A). This observation is consistent with previous reports linking elevated HP1 levels to poor prognosis in HCC (Supp. Fig. 6B).

Patients were next ranked according to their cumulative HP1 expression, calculated as the sum of CBX3, CBX1, and CBX5 expression, and stratified into two groups representing the upper and lower quartiles (Hi HP1 and Lo HP1, respectively; Fig. 6A; Sup Fig. 6C). This classification effectively separated the patients into two distinct subgroups in an unsupervised PCA analysis (Fig. 6B). Notably, the Hi HP1 group was enriched for patients previously associated with poor prognosis and included a higher proportion of deceased individuals (Fig. 6A; Supp. Fig. 6D–E; (Candia *et al*, 2020).

As the available transcriptomes lacked sufficient depth to detect rare unstable RNAs originating from enhancers or promoters, we estimated global RNA degradation activity by quantifying the accumulation of unstable mRNAs using the RNA HiLo ratio, a previously validated measure of rare RNA accumulation (Mullani *et al*, 2021). This analysis revealed that labile mRNA species accumulated significantly more in Lo HP1 tumors compared to Hi HP1 tumors (Fig. 6C). Moreover, genes involved in antiviral defense mechanisms, including RIG-I, NLRP3, ISG20, and IRF7, were expressed at significantly higher levels in the Lo HP1 tumors (adjusted p-values: 0.00108, 0.000000249, 0.000000709, and 0.0000544, respectively; Fig. 6D), suggesting an innate immune response triggered by the accumulation of aberrant RNA species. Gene ontology (GO) analysis revealed that genes upregulated in Hi HP1 tumors were significantly enriched (adjusted p-value 4.87E-14) for the KEGG pathway associated with cell cycle regulation (Supp. Fig. 6F). This finding correlated with increased expression of alpha-fetoprotein and YAP1, markers indicative of de-differentiated and highly proliferative hepatocytes (Fig. 6D). Taken together, these data indicate that Hi HP1 tumors are, on average, poorly differentiated, highly proliferative, and more aggressive.

In Lo HP1 tumors, we observed upregulation of genes expressed predominantly in immune cells rather than hepatocytes, suggesting substantial immune infiltration. Furthermore, Lo HP1 tumors exhibited increased expression of alpha-smooth muscle actin (α-SMA/ACTA2) and vimentin, markers of activated hepatic stellate cells (HSCs) (Fig. 6D). Notably, GO cellular component analysis identified "collagen-containing extracellular matrix" as the best scoring pathway, consistent with our observations in the mouse liver cells with reduced RNA exosome activity (Fig. 6F, 5D). These findings suggest that Lo HP1 tumors promote a fibrotic evolution of the tumor microenvironment (Summarized in Fig. 6G). They further imply that the increased expression of collagen-associated genes may be a direct consequence of reduced HP1/RNA exosome activity on chromatin, and that these genes are particularly sensitive to enhancer regulation dependent on chromatin-linked RNA degradation mechanisms.

Discussion

We have identified here a novel relationship between the chromatin-associated HP1 proteins and the functionality of the nuclear RNA exosome. HP1 proteins are required for proper targeting of the complex to chromatin loci. Their depletion in BMEL cells increased the stability of several nuclear RNA species, such as transcripts produced at repeated loci, promoters and enhancers. Many HP1-associated enhancers showed increased transcriptional activity after loss of HP1. These activated enhancers have an impact on the expression of certain extracellular matrix components such as Collagen genes, with important functional consequences in the context of hepatocellular carcinoma.

HP1 depletion phenocopies RNA Exosome depletion in the regulation of targeted transcripts

The spectrum of dysregulated RNA species upon HP1 invalidation in BMEL cells recapitulates the effects resulting from the depletion of nuclear exosome complex components described in the literature. Levels of short-lived nuclear RNAs increased in TKO BMEL cells in our study, and in cells depleted of NEXT or PAXT components in several other studies. PROMPTs and eRNAs increased compared to genic transcripts upon depletion of RRP40/EXOSC3 (core exosome) or ZCCHC8 (NEXT) (Lubas *et al*, 2015). Depletion of ZFC3H1, a PAXT component, resulted in an upregulation of the same set of nuclear RNAs than those targeted by the NEXT complex, even though PAXT was found to target preferentially polyadenylated forms of these RNAs (therefore at a later transcript maturation stage) (Meola *et al*, 2016). The correlation of dysregulated RNA species between HP1-depleted cells and the depletion of NEXT and PAXT components suggests that HP1 affects the functionality of nuclear exosome complexes towards their RNA targets.

Contrary to these previous studies, our strategy in BMEL cells did not involve the depletion of exosome components or some of its nuclear cofactors. Indeed both RNA and protein levels of the components analyzed so far were not significantly affected between Het and TKO BMEL clones. Despite this, activity of the nuclear exosome complex appeared to be impaired in its capacity to degrade chromatin-associated RNA. The local association of exosome components onto chromatin as revealed by the number of ChIPseq peaks was drastically lost in the absence of HP1. But these components were not globally released from the chromatin fraction, clearly demonstrating that HP1 drives the exosome components towards specific hot-spots and the complex is delocalized from specific chromatin loci without HP1. HP1 proteins are highly mobile in the nucleus as demonstrated by photobleaching experiments that suggested a dynamic HP1 binding as a mechanism of heterochromatin maintenance (Cheutin *et al*, 2003; Festenstein *et al*, 2003). We have previously observed that HP1gamma associates with pre-messenger transcripts on chromatin primarily at introns, and peaks of RNA binding by HP1 were found correlated with active chromatin marks rather than H3K9me2/3-enriched loci (Rachez *et al*, 2021). In line with this, single-molecule experiments comparing recruitments of all three human HP1 generated a dynamic model where the most common HP1 associations involves charge-dependent DNA interactions, enabling rapid transitions between a free form and DNA- and nucleosome-binding states (Bryan *et al*, 2017). DNA and RNA may be interchangeable in this process. These properties are then reminiscent of the dynamic binding cycle of Swi6 in S. pombe in the silencing of

pericentromeric Satellite repeat RNA, by directing RNA to the poly(A) polymerase Cid14 for degradation by the exosome. (Keller *et al*, 2012). In the context of our results, a dynamic exchange of HP1 proteins between H3K9me3 nucleosomes and nucleic acids may explain its key role in providing chromatin accessibility to the RNA exosome at many diverse genomic loci well beyond the constitutive heterochromatic domains. We may view HP1 as a factor providing or restricting chromatin accessibility thereby allowing the RNA exosome to find its RNA substrates.

HP1 and retroelement transcript silencing : transcriptional repression and RNA degradation

The TKO-specific transcripts detected at a subset of LTRs in the absence of HP1 are linked to a dysregulation of the RNA exosome. LTRs are also typical heterochromatin loci, since transposable elements (TEs) are transcriptionally inactive in most mammalian cells. They are transcriptionally silenced by several pathways. While DNA methylation is thought to be the dominant suppressive mechanism in somatic tissues and late embryos, TEs are suppressed by H3K9me3-dependent mechanisms in embryonic stem cells, essentially at the more potentially active, evolutionarily younger retroelements (Bulut-Karslioglu *et al*, 2014). In the yeast *S. pombe*, heterochromatic gene silencing is ensured by two different HP1 homologs. Chp2 associates with the SHREC histone deacetylase complex and mediates transcriptional repression by RNA polymerase II, while Swi6 associates with noncoding centromeric transcripts and is required for efficient degradation of these transcripts, by an RNAi-dependent machinery or by the RNA exosome (Keller *et al*, 2012; Motamedi *et al*, 2008). In mESC the human silencing hub (HUSH) complex contributes to TE silencing. This complex is recruited to H3K9me3-enriched nucleosomes via its MPP8 component. The HUSH complex cooperates with RNA degradation machineries, including the NEXT complex in the repression of TEs (Garland *et al*, 2022; Matkovic *et al*, 2022).

We cannot rule out that a loss of transcriptional repression may contribute to the nuclear accumulation of LTR-derived transcripts in the absence of HP1. However, the loci of detectable LTR transcripts in BMEL cells did not match any of the loci enriched in MPP8 recruitment by ChIP-seq in mESC from Garland et al. (Supp. Fig. 3C-E). Despite the different cell lines involved, comparison of these data suggested no obvious implication of the HUSH complex in transcriptional repression in this context. This does not exclude the contribution of other machineries, such as, TNRC18, an H3K9me3 reader that is involved in the epigenetic silencing of evolutionarily young ERV loci (Zhao *et al*, 2023). Since HP1 proteins are chromatin silencing factors, the increased RNA levels we observed in TKO cells may very well result from a dual impact of HP1 proteins on both the loss of transcriptional repression and an impaired RNA degradation mechanism, reminiscent of the combinatorial impact of HUSH and NEXT machineries in mESCs, or SHREC and RNA degradation machineries in yeast. This hypothesis awaits further investigation.

Exaptation of LTRs co-opted as enhancers

Despite the fact that they have lost the ability to transpose in mammalian genomes, retroelements such as LTRs bear within their sequence, because of their viral origin, many transcription regulatory elements which constitute a platform for transcription factor access and transcription initiation. They may thereby affect a number of gene regulatory mechanisms (Fueyo *et al*, 2022). Retroelements may be co-opted as alternative promoters, enhancers, or chromatin

insulators at CTCF binding sites. Many LTR sequences derived from distantly related ERVs have been exapted as regulatory sequences for many genes in a wide range of mammalian tissues. A previous study in our model of BMEL cells has described several examples of LTR exaptation as enhancers (Calvet *et al*, 2022). We also previously described how increased transcription of endogenous retroviruses (HERVs) in multiple sclerosis may correspond to reactivation of HERV-derived embryonic enhancers (Azebi *et al*, 2019).

The few thousand LTR derived transcripts that we found significantly stabilized in TKO cells may contribute to the mechanisms leading to transcriptome dysregulation in BMEL cells. In this respect, co-opted LTRs are known to constitute a source of long non-coding RNAs (lncRNA). Such accumulation of non-degraded nuclear RNA may affect chromatin structure and cellular processes. Enhancer RNA (eRNA) is a hallmark of active enhancers, but it is still debated whether transcription at enhancer or eRNA molecules themselves are key to their activity: eRNA may act by promoting chromatin accessibility at enhancers, but eRNA may also modulate the chromatin association of transcriptional regulators, such as transcription factors, coactivators, and regulators of the RNA polII elongation process (for a review: (Sartorelli & Lauberth, 2020). Such a mechanism may explain the increased levels of phosphorylated RNA polII in TKO cells through eRNAs promoting RNAPII elongation by acting as a decoy for the negative elongation factor NELF and contributing to the activation of P-TEFb (Schaukowitch *et al*, 2014).

Impact of Exosome dysregulation on transcriptional programs in HCC

The triple HP1 invalidation in mouse liver has revealed previously that HP1 depletion leads to the development of liver tumors in old animals with a higher incidence than in control mice, associated with a significant overexpression of several genes frequently dysregulated in human HCC, including *Trp53* (Saksouk *et al*, 2020). These results correlate with HP1 proteins being a prognostic factor associated with human liver cancer (supp. Fig. 6B). EXOSC10 has also a predictive value for the prognosis of HCC and may regulate the progression of HCC through the p53-related signaling pathways (Meng *et al*, 2023). Our BMEL cells provide an appropriate model for the analysis of cancer progression where it is often the accumulation of mutations in resident stem cells in a tissue which is the origin of carcinogenesis. We found genes involved in collagen extracellular matrix formation to be particularly sensitive to reduced RNA exosome activity. Both reduced HP1 expression and reduced RNA exosome activity seemed to contribute to increased expression of these genes. The exact mechanism underlying this specificity remains unclear. However, previous studies have shown that certain enhancer RNAs (eRNAs) and long noncoding RNAs (lncRNAs) are particularly susceptible to RNA exosome-mediated degradation and tend to accumulate upon its inactivation (Pefanis *et al*, 2015). Consistent with this, we have found chromatin-enriched RNA in BMEL cells to be accumulated in the absence of HP1 on enhD and PROMPTs, two categories corresponding to eRNAs and a subset of lncRNAs, respectively. As mentioned previously, these RNA species are suspected to play regulatory roles in gene activation, they may be inducing transcriptional activity by altering chromatin three-dimensional structure or by promoting elongation through neutralization of NELF. An alternative explanation is that collagen genes are highly regulated at the mRNA stability level (as reviewed by (Zhang & Stefanovic, 2016). Supporting this hypothesis, we observed an overall enhanced stabilization of otherwise labile mRNAs in the Lo HP1 patients, potentially due to reduced RNA turnover.

Experimental Procedures

Cell lines

Het and TKO cells (Het 1, Het 3.2, Het 3.5, TKO1, TKO2, TKO3), as described in Figure 1A, were independent clones of BMEL cells derived from mouse embryonic liver, generated as previously described (Saksouk et al., 2020). The cells were cultured in RPMI 1640 medium (Invitrogen) supplemented with 10% fetal bovine serum (FBS), 1% penicillin-streptomycin, 10 µg/mL insulin, 30 ng/mL IGF-II, and 50 ng/mL EGF, at 37 °C under 5% CO2.

Cell fractionation and total cell extracts

Cells (approximately 10^6 from a confluent 100 mm plate) were washed twice with ice-cold PBS directly on the plate then incubated on ice for 8 minutes in 10 mL of swelling buffer (SW): 10 mM Tris-HCl pH7.5, 2 mM MgCl2, 3 mM CaCl2, supplemented before use with 1x antiprotease (Roche), 0.5mM Na3VO4, 20mM beta-Glycerophosphate, 0.1mM DTT, 1U/ul RNasin (Promega). Cells were removed from the plate by scraping, and pelleted by centrifugation at 1600 rpm for 5 minutes at 4°C. Cell pellets were resuspended in 400 µL of lysis buffer (SW buffer containing 10% glycerol and 0.1% NP-40) and gently pipetted up and down 15 times using a P1000 tip and centrifuged at 2500 rpm for 5 minutes at 4°C to pellet the nuclei. The supernatant was considered as the cytosolic fraction. Nuclear pellets were resuspended in 400 µL of RB buffer containing 9 mM EDTA, 0.2 mM EGTA, 0.1% Triton X-100, supplemented before use with 1x antiprotease (Roche), 0.5mM Na3VO4, 20mM beta-Glycerophosphate, 1mM DTT, 1U/ul RNAsin (Promega) incubated for 15 minutes while rotating at 4°C, and centrifuged at 3000g for 5 minutes to pellet chromatin. The supernatant was considered as the nucleosolic fraction. Chromatin pellet were resuspended in 400 µL of RB buffer supplemented with 1% SDS and solubilized by sonication using a water bath sonicator (Diagenode Bioruptor) at high amplitude (6 cycles of 20 seconds). In parallel, total cell extracts were prepared in RIPA buffer: 150 mM NaCl, 50 mM Tris pH 8, 0.25% sodium deoxycholate, 0.1% SDS, 1% NP-40, freshly supplemented with 0.5 mM DTT and 1× protease inhibitor, RNAsin then incubated for 10 minutes on ice.

Co-immunoprecipitation assays

Approximately 10^6 cells from a confluent 100 mm plate were used to prepare nuclei according to the cell fractionation protocol described above. Nuclear pellets were resuspended in 0.5 ml of RIP buffer: 25mM TRIS pH 7.4, 150mM KCl, 2.5% glycerol, 0.3% NP-40 freshly supplemented with 1x antiprotease, 0.5 mM Na3VO4, 20mM beta-glycerophosphate, 0.1 mM DTT, 1U/ul RNAsin, and treated with 7U/mL TURBO DNase. The suspension was incubated at 37°C for 5 minutes. Samples were sheared by three cycles of sonication (10 seconds ON, 10 seconds OFF) using a Diagenode Bioruptor, followed by a second incubation at 37°C for 5 minutes. The reaction was stopped by addition of 10 µl /mL of 0.5M EDTA per 0.5 ml. Samples were then centrifuged at 12000g for 10 minutes at 4°C. The resulting supernatant, referred to as "RIP extract", was used for subsequent immunoprecipitation (IP) experiments, and a portion of the RIP extract was reserved as input samples.

For each IP, 150 µl of RIP extract was combined with 3 µg of antibodies and 350 µl of RIP buffer. The mixture was incubated for 1h30 at 4°C on a rotating wheel. Saturated magnetic beads (Dynabeads M-280 Sheep Anti-Rabbit IgG or Dynabeads Protein G, Invitrogen) were prepared by blocking 80 µl of beads per IP in PBS supplemented with 0.1% BSA, 0.5% NP40, and 0.1% polyvinylpyrrolidone (PVP) for 30 min at 4°C, followed by two washes with Wash V buffer: 0.1%

NP-40, 150mM NaCl, 20 mM TRIS.Cl pH8, 1mM EDTA. The saturated beads were resuspended in 300 µl of Wash V buffer per IP, and added to the IP mixture. After 45 minutes of incubation, beads were then washed twice with RIP buffer, twice with Wash V buffer, and once with TE/NP40 buffer: 10 mM TRIS pH7.4, 1 mM EDTA, 0.01 % NP-40. Beads were eluted in Laemmli sample buffer. Both eluates and input samples were further processed for Western blot analysis.

Cell fractionation for RNA preparation and sequencing (RNAseq)

For total RNA extraction, cells were trypsinized, and the resulting pellet was washed with PBS, and pelleted by centrifugation at 1800 rpm for 4 minutes at 4°C. The cell pellet was resuspended in 1600 µL of Buffer D: 4 M guanidinium thiocyanate, 25 mM sodium citrate, pH 7.0, 0.5% (wt/vol) N-laurosylsarcosine and 0.1 M 2-mercaptoethanol (Chomczynski & Sacchi, 2006), homogenized thoroughly for total cell extracts, from which the total RNA was extracted.

For chromatin-associated and cytosolic RNA extraction, cells were resuspended, as described above for cell fractionation, in 125 µL of ice-cold SW buffer and incubated on ice for 8 minutes. After swelling, 125 µL of lysis buffer was added, and the suspension was gently pipetted 15 times before centrifugation at 3500 rpm for 4 minutes at 4°C. The nuclei pellet was resuspended in 250 µL of Buffer RB and incubated on ice for 15 minutes, followed by centrifugation at 6000 rpm for 4 minutes at 4°C, separating the chromatin and nucleosol. Both the nucleosol and chromatin fractions were homogenized in Buffer D for RNA extraction.

RNA was extracted by addition to all fractions of 250 mM sodium acetate, 1 volume of acidic phenol, and 0.2 volumes of chloroform. The samples were incubated on ice for 10 minutes, followed by centrifugation at 14,000 g for 20 minutes at 4°C. The supernatant was collected and mixed with an equal volume of chloroform, then centrifuged at 14,000 g for 5 minutes at 4°C. The resulting supernatant was combined with an equal volume of isopropanol, vortexed thoroughly, and incubated overnight at -20°C for RNA precipitation. The samples were centrifuged at 14,000 g for 20 minutes at 4°C, and the resulting pellet was washed with 75% ethanol. The pellet was resuspended in 100 µL of Buffer D (diluted 1:10), supplemented with 0.5% Triton X-100, 0.4 M NaCl, and 1 µL of proteinase K. The mixture was incubated at 50°C with shaking at 850 rpm for 3 hours. Subsequently, 250 mM sodium acetate, 300 µL of Buffer D, and 400 µL of acidic phenol/chloroform were added to each fraction. The samples were centrifuged at 14,000 g for 15 minutes at 4°C, and the supernatant was collected. An equal volume of chloroform was added to the supernatant, followed by centrifugation at 14,000 g for 20 minutes at 4°C. The final supernatant was supplemented with Glycogen (2 µg/µL) as carrier and 1 volume of isopropanol, and the samples were precipitated overnight at -20°C. The pellet was then washed with 75% ethanol and resuspended in 50 µL of RNase-free water. The samples were incubated at 45°C with shaking at 800 rpm for 10 minutes. 40 µL was subjected to DNase treatment for 50 minutes at 37°C. RNA integrity was verified by agarose gel electrophoresis. On all RNA fractions, total RNA library preparation and sequencing were performed by Novogene (UK) Co., Ltd as part of their lncRNA-seq service, which included directional library preparation with rRNA removal and sequencing on the Illumina NovaSeq platform using paired-end 150 bp (PE150) reads.

Chromatin immunopreciptation and sequencing (ChIPseq)

BMEL cells were crosslinked following a modification of the protocol by (Festuccia *et al*, 2016). Briefly cells were incubated in freshly prepared 2 mM DSG (Merck) in PBS for 50 minutes at room temperature with occasional shaking. After three washes in PBS, cells were incubated for

10 minutes in 1% formaldehyde (Merck) in PBS. The crosslinking reaction was quenched with 125 mM glycine for 5 minutes at room temperature. Cells were washed with PBS, harvested, and pelleted by centrifugation at 3000 g for 3 minutes. Cells were subsequently resuspended in 1.4 mL of freshly prepared swelling buffer (25mM Hepes pH 7.95, 10mM KCl, 10mM EDTA) supplemented with protease inhibitors (Roche) and 0.5% NP-40. The suspension was incubated on ice for 30 minutes, then pipetted up and down 50 times using a P1000 pipette tip. The cells were centrifuged at 6000g for 2 minutes and resuspended in 300 µL of TSE150 buffer with 0.3 % SDS (0.3% SDS, 1% Triton, 2mM EDTA, 20mM Tris-HCl pH8, 150mM NaCl) freshly supplemented with protease inhibitors. Chromatin was sonicated in 1.5 mL tubes for a total of 15 minutes using cycles of 30 seconds ON and 30 seconds OFF, with the samples maintained in ice-cold water. Following sonication, the samples were centrifuged at 14,000g for 30 minutes at 18°C. An aliquot of supernatant was used to quantify chromatin and check DNA fragment size (typically around 300 bp).

Chromatin immunoprecipitation (ChIP) was performed using 70 µg of chromatin and 4 µg of the following antibodies : anti-MTR4/SKIV2L2 (Bethyl A300-615A), anti-ZC3H18 (Atlas HPA 040847), anti-EXOSC10 (Bethyl A303-987A), anti-CTCF (Diagenode A2354-0023P), anti-P-RNAPII (a mix of antibodies against phospho-Ser5 and phospho-Ser2, Abcam Ab5095 and Ab5408, respectively), and anti-murine IgG (Merck). Immunoprecipitation was carried out overnight on a rotating wheel at 4°C. Subsequently, 90 µL of Protein G beads (Dynabeads, Invitrogen), blocked overnight at 4°C in blocking buffer containing 5% Buffer C (0.5% SDS, 10 mM Tris-Cl pH 8, 1 mM EDTA, 0.5 mM EGTA), 20% Buffer D 1.2× (1.2% Triton, 0.12% NaDoc, 180 mM NaCl, 12 mM Tris-Cl pH 8, 1.2 mM EDTA, 0.6 mM EGTA), 72% Wash Buffer V, 1.5% BSA (Merck), and 1.5% Polyvinylpyrrolidone (Merck), were added to the IP samples. Ten percent of the chromatin was set aside as input. Following immunoprecipitation, the beads were pelleted and subjected to sequential washes, each performed for 3 minutes on a rotating wheel at room temperature using 1 mL of the following buffers: Three washes in TSE150 buffer with 0.1 % SDS (0.1% SDS, 1% Triton, 2mM EDTA, 20mM Tris-HCl pH8, 150mM NaCl), then one wash in TSE500 buffer (TSE150 buffer with 0.1% SDS and 500 mM NaCl), then one wash in buffer (10 mM Tris-HCl pH 8, 0.25 M LiCl, 0.5% NP-40, 0.5% sodium deoxycholate, 1 mM EDTA), then two washes in TE buffer (10 mM Tris-HCl pH 8, 1 mM EDTA). Elution was performed in 300 µL of elution buffer (1% SDS, 10 mM EDTA, 50 mM Tris-HCl pH 8) by vortexing vigorously, followed by incubation at 65°C for 15 minutes. A second elution was performed using 100 µL of elution buffer. Both eluates were collected, and the beads were rinsed in 100 µL of TE buffer with 1% SDS, subsequently added to the pool of eluates. Both the immunoprecipitated and input chromatin samples were incubated overnight at 65°C to reverse crosslink, followed by proteinase K and RNase A treatments. DNA was isolated using a NucleoSpin PCR purification kit (Macherey Nagel), and concentrations were measured using a Qubit fluorometer (Invitrogen). Purified ChIP samples were processed for Illumina paired-end (PE40) sequencing performed at the Genom'IC core facility (Paris, France).

Western Blotting analysis

Protein samples were denatured by the addition of Laemmli sample buffer (Bio-Rad) with reducing agent at 100°C for 10 minutes and separated by SDS-PAGE (Bio-Rad, Criterion XT), then transferred to a nitrocellulose membrane. Transferred proteins were visualized by Ponceau S staining, and the membranes were incubated overnight at 4°C in PBS-T (PBS, 0.1% Tween 20), containing 5% (w/v) non-fat dry milk. The membranes were then incubated for 1h30 at room

temperature with primary antibodies at the appropriate dilution in PBS-T (as described in the Western blot antibodies section). After three 5-minute washes in PBS-T, the membranes were incubated for 1h30 with secondary antibodies (Starbright Blue 700 anti-rabbit/mouse IgG (Biorad), or rabbit true blot (Rockland), all diluted 1/4000), followed by three additional 5-minute washes. Protein detection was performed either by fluorescence at 700 nm or by chemiluminescence using the Pierce™ ECL Plus Western Blotting Substrate (Thermo Fisher Scientific) and visualized with a ChemiDoc MP imaging system (Bio-Rad).

Western blot antibodies

Antibodies	Dilution	References
Anti-EXOSC3	1/1000	Proteintech 15062-I-AP
Anti-EXOSC9	1 /1000	Abcam ab156686
Anti-EXOSC10	1/1000	Bethyl A303-987A
Anti-DIS3L	1/300	Atlas HPA041805
Anti-MTR4/SKIV2L2	1 /1000	Bethyl A300-615A
Anti-ZC3H18	1 /2000	Bethyl A304-682A
Anti-CTCF	1/1000	Diagenode A2354-0023P
Anti-HP1α	1 /1000	Euromedex 2G9
Anti-HP1β	1/2000	Euromedex 1A9
Anti-HP1γ	1/3000	Euromedex 1G6
Anti-H3K9me3	1/2000	Abcam ab8898
Anti-H3K27me3	1/2000	Cell Signaling Technol. CST-9733

ATACseq

Chromatin accessibility assays were performed on each of the six Het and TKO BMEL clones according to the protocol by (Buenrostro *et al*, 2013), with an ATACseq kit (ActiveMotif, 53150). Paired-end (PE40) sequencing of the dual-index ATACseq libraries was performed by Novogene (UK) Co., Ltd.

CUT&Tag

CUT&Tag assays were performed on two independent biological replicates of Het and TKO BMEL cells according to the protocol by (Kaya-Okur *et al*, 2019), but with the NE1 buffer (https://www.protocols.io/view/bench-top-cut-amp-tag-kqdg34qdpl25/v3) to permeabilize cells, and with the same anti-HP1α, -HP1β, -HP1γ, -H3K9me3 as used in Western blot analyses, and with anti-H3K27me3 (Cell Signaling Technol. 9733). Libraries were obtained with 15-16 PCR amplification cycles such that at least a faint ladder of nucleosome-sized bands were visible using an Agilent Tape Station High-Sensitivity D1000 Screen Tape representing DNA concentrations of at least 200 pg/µl for anti-HP1 CUT&Tag reactions with Het cells, and at least 10-fold lower concentrations for the same reactions using TKO cells. 40 nt paired-end sequencing was performed at the I2BC sequencing platform. Reads were aligned on the mm10 reference genome with bowtie2 (parameters: --end-to-end --very-sensitive --no-mixed --no-discordant -k 1 -X 1000 --phred33 -I 25 -p 24 -x mm10). Bigwig files were generated from two merged HP1 CUT&Tag replicates, and they were normalized using CPM.

Bioinformatics analyses

RNAseq data analysis : Mapping was carried out with STAR (v2.6.0b) (parameters: –outFilterMismatchNmax 1 – outSAMmultNmax 1 –outMultimapperOrder Random –outFilterMultimapNmax 30). The reference genome was GRCm38 Mus musculus primary assembly from Ensembl. The SAM files were converted to BAM files and sorted by coordinate using samtools (v1.7). Gene expression analysis was performed with the DESeq2 (v1.18.1) package. P-values from the differential gene expression test were adjusted for multiple testing according to the Benjamini and Hochberg procedure. Bigwig files were generated from .bam files with bamCoverage (parameter: –normalizeUsing CPM) from Deeptools (v3.1.3).

ChIPseq and ATACseq data analysis : Reads were mapped to the mm10 reference genome assembly using STAR and Bowtie2. ChIPseq peaks were identified with MACS2 version 2.1.1.20160309, with FDR < 0.05.

Definition of genomic regions and categories

LTR, SINE, LINE, and MMSAT regions were defined by the RepClass field in the Repeat masker database in the UCSC table browser (https://genome.ucsc.edu/). The enhD Distal enhancers were defined as the dELS/enhD category in the Encyclopedia of DNA Elements (ENCODE) candidate cis-regulatory element (cCRE) database in the UCSC table browser. Extragenic repeats and enhD elements were defined relative to genes in the Ensembl Grc38 database (https://www.ensembl.org/). Promoter associated transcripts (PROMPT) regions were defined as 2kb upstream of transcription start sites (TSS) of genes. Exons were defined according to the Ensembl Grc38 database. The list of 23808 Genes was defined according to the Ensembl Grc38 database, after removing all the entries with names beginning with "Mir", "Rik", and "Gm", for the sake of clarity of the average density profiles.

The EnhD (Up, Down, Unchanged, and Closed) categories were created according to their activity as defined by ATACseq read counts obtained by featurecounts on distal enhancer elements (enhD) in ENCODE database. EnhD categories are as follows :

enhD Up (ATACseq reads>10 p-val.<0.05 FC TKO vs. Het >=4),
enhD Down (ATACseq reads >10, p-val.<0.05 FC TKO vs. Het <= 0.25),
enhD Unchanged (ATACseq reads >10, 0.9<FC<1.1),
enhD Closed (ATACseq reads <2).

RNA Read counts on genomic regions

Quantification of uniquely mapped reads from the transcriptome was carried out with featureCounts (v1.6.1) from the Subread suite (Liao et al., 2014), with the following parameters: -p -B -C -s 1 --minOverlap 25. FeatureCounts with these parameters counted only uniquely mapped reads with both paired-ends aligned (-p -B).

Chromatin and cytoplasmic stranded RNA reads were counted on extragenic repeats only in order to evaluate self-expressed repeats and avoid counting reads on gene-embedded repeats which would reflect expression of the surrounding gene and not the repeat itself. Read counts were substracted by stranded reads counted in the 200nt region upstream of repeats adjusted for their size.

Transcriptome reads on PROMPT were counted antisense, corresponding to upstream-antisense RNA (uaRNA), relative to the orientation of their adjacent gene substracted by antisense

read counts in its first exon adjusted for their respective size. Transcriptome read counts on enhD were substracted by read counts in the highest of the two adjacent 200nt region upstream or downstream of each enhD adjusted for their respective size. All genomic regions counted for RNA levels were considered expressed when two or more reads were counted in average of the triplicate samples, in either Het or TKO or both, after substracting reads from size-normalized adjacent regions (illustrated in Figures 2B and 2E). In order to avoid excluding the elements expressed only in Het or in TKO, a pseudocount of 0.1 was added to the mean RNA read counts before transformation into Log2 (illustrated in Figures 2C, 2D, 2F and 2G).

Data visualization

BigWig files of samples or merged replicates were visualized with the Integrative Genomics Viewer (IGV version 2.8.10). Heatmaps and profiles were generated with the computeMatrix, plotProfile and plotHeatmap tools of the Deeptools package (v3.1.3).

Data availability

All RNA-seq, ChIP-seq, ATAC-seq, and CUT&Tag datasets generated during this study are available at the Gene Expression Omnibus (GEO) under accession code GSE000.

Acknowledgments

The authors wish to thank the technical help of Enzo Becherel. This work has been supported by PhD fellowships from La Ligue Nationale Contre le Cancer (to HS) and by grants from Aviesan ITMO Cancer (Plan Cancer) and Institut National du Cancer (INCA).

We acknowledge the sequencing and bioinformatics expertise of the I2BC High-throughput sequencing facility, supported by France Génomique (funded by the French National Program "Investissement d'Avenir" ANR-10-INBS-09).

Conflict of Interest Statement

The authors declare that they have no conflict of interest.

Figure legends

Figure 1: Protein-protein association between HP1 and the RNA Exosome.
A. String analysis of factors co-precipitating with ZC3H18 proteins, identified by interaction profiling of ZC3H18, in Winczura et al., 2018. **B.** Genotype and subcellular fractionation scheme of the six BMEL clones expressing (Het) or not (Triple Knock-out, TKO) HP1 proteins used in this study. **C.** Protein levels in total extracts, and **D,** subcellular distribution in the three fractions, cytosolic (C), nucleosoluble (N), and chromatin (X), depicted in Figure 1B of indicated exosome subunits and cofactors in Het and TKO cells by Western blot analysis and Ponceau staining of total proteins. **E, F, G.** Co-immunoprecipitation of HP1γ by MTR4, ZC3H18, EXOSC10, or EXOSC9 in the nuclear fraction.

Supplementary Figure 1: A. Levels of HP1 proteins in all BMEL clones by Western blot analysis. **B.** Distribution of indicated proteins in the subcellular fractions (C, N, X, as in Fig. 1B) in two representative Het and TKO clones by Western blot analysis, and total proteins by Ponceau S staining. **C**. Genome views as in Figure 2A of the distribution of RNA density profiles between cytosolic and chromatin fractions for Actb mRNA and the nuclear Malat1 RNA or U-snRNA. Distribution reflects the expected subcellular localizations of the depicted RNA species. **D, E.** Co-immunoprecipitation assays of HP1α, HP1β, and HP1γ by MTR4, ZC3H18, or EXOSC9, compared to IgG. **F.** RNA-independent co-immunoprecipitation of HP1γ by ZC3H18 and EXOSC9. HP1γ signal is not lost upon RNase A treatment.

Figure 2: Chromatin-enriched RNA is increased in TKO cells and stabilized in the cytoplasm**.**
A. Genome views of RNA density profiles (merged triplicates) in chromatin (green) and cytosolic (red) fractions, at indicated genomic loci showing TKO-specific or TKO-increased RNA. **B, C, D.** RNA levels by counting uniquely mapped reads on repeat elements (LTR, LINE, SINE, MMSAT4), Promoter upstream antisense RNA (PROMPT), and distal enhancers (enhD) are increased in TKO chromatin, but remain mostly unchanged on exons of genes in Ensembl database. **B.** Cumulative histograms of proportions of the indicated genomic regions expressing RNA (more than 2 reads) by comparison of the three Het clones with the three TKO clones. Five categories discriminate expression on chromatin in TKO only (brown), increased in TKO (salmon), in Het only (dark blue), increased in Het (light blue), unchanged (grey). **C, D.** Boxplots of mean RNA read counts in chromatin (C) or in the cytosol (D) on genomic regions as in B. in Het (blue) or TKO (orange). **** $p < 0.0001$, *** $p < 0.001$, ** $p < 0.01$, * $p < 0.05$, n.s., not significant (unpaired two-tailed Student's t-test). **E, F, G.** Histogram and boxplots as in figures B, C, D, for proportions and counts on expressed exons (more than 10 reads). **H.** Transcriptome profiles in Het or TKO chromatin (green) or cytoplasm (red) compared with transcriptomes of mESC invalidated for the expression of NEXT or PAXT Exosome complex components, *Zcchc8* KO (sky blue profiles) or *Zfc3h1* KO (yellow profiles) and control mESC (grey profiles) (GSE178550; Garland et al., 2022).

Figure 3: ChIPseq analysis reveals an HP1-dependent targeting of Nuclear RNA exosome and cofactors to chromatin loci.
A. Genome views of chromatin RNA density profiles (top), ChIPseq profiles of indicated proteins, and HP1 CUT&Tag density profiles (bottom) on indicated loci. **B.** Number of ChIPseq peaks versus IgG defined by MACS2 analysis for the indicated proteins in Het32 (blue) and TKO2 (brown). **C.** Heatmaps of genome-wide ChIPseq densities centered on ChIPseq peaks in both Het32 and TKO2 combined in a single list (all peaks). **D.** Metagene analysis of ChIPseq profiles of the indicated proteins on 23808 gene bodies defined as TSS to TES intervals, in Het32 (dark blue), in TKO2 (dark red), compared to IgG profiles in Het32 and TKO2 (salmon and light blue profiles, respectively). **E.** CUT&Tag profiles at gene TSS for the three HP1 proteins (E) in Het (blue profiles), and HP1α in TKO (salmon profile). **F.** Cut&Tag profiles at TSS for H3K9me3 (purple) and H3K27me3 (brown) histone marks in Het (dark colors) and in TKO (light colors).

Supplementary Figure 3: A, B. Heatmaps of densities of H3K9me3 or HP1 isoforms by Cut&Tag in Het or TKO as indicated, on gene bodies (A) as in figures 3D-F, or on a list of simple repeats (B) from Repeat Masker database. **C, D.** Genome views of transcriptomes in Het or TKO (examples depicted in figure 2H) compared with transcriptomes of mESC invalidated for the expression of *Zcchc8* KO (sky blue profiles) or *Zfc3h1* KO (yellow profiles) and control mESC (grey profiles), together with MPP8 chIPseq (red) and input (dark red) profiles (GSE178550; Garland et al., 2022). **C.** Genome views of two examples of MPP8 ChIPseq peaks with a coincidental RNA profile in mESC KO. No upregulated RNA was detectable at these loci in Het or TKO. **D.** Genome views of upregulated RNA (green and red) in TKO at LTR loci, with a coincidental upregulated RNA in mESC KO (yellow and sky blue). No MPP8 ChIPseq peak was detectable at these loci. **E.** MPP8 duplicate chIPseq (orange and red) and input (dark red) profiles at LTR loci sorted in three categories based on their cell-type specificities, as in Figure 2B (GSE178550; Garland et al., 2022).

Figure 4: HP1-dependent CTCF and MTR4 at promoters.
A. Number of MTR4 peaks (purple bars) colocalized with the other indicated ChIPseq peaks, compared to the same list of MTR4 peaks with randomized genomic locations (gray bars). **B,** Number of CTCF ChIPseq peaks versus IgG defined by MACS2 analysis in Het32 (blue) and TKO2 (brown). **C.** Genome view of chromatin-enriched RNA, CTCF and MTR4 densities at a locus showing two regions bearing TKO-only CTCF peaks (on the left), or peaks common to both cell types (on the right). **D.** Heatmaps of genome-wide CTCF ChIPseq densities in Het32 and TKO2 centered on all CTCF ChIPseq peaks. **E.** Heatmaps of ChIPseq densities of the indicated proteins on 23808 gene bodies defined as TSS to TES intervals, in Het32 (dark blue), in TKO2 (dark red).

Figure 5: Changes in chromatin accessibility at enhancers affect collagen gene expression.
A. Number of CUT&Tag HP1 merged peaks located at cCRE regulatory elements annotated as in Supp. Fig. 5A. **B.** Heatmaps of ATACseq densities in Het and TKO cells, and of HP1alpha CUT&Tag densities in Het cells centered at cCRE enhD enhancer regulatory elements. EnhD were categorized based on their chromatin accessibility by ATACseq between Het and TKO. Categories are as follows: Down, with decreased accessibility in TKO cells; Unchanged, active in both conditions; Up, with increased accessibility in TKO cells; inactive (not shown), with no ATACseq density, respectively. **C.** Proportions of expressed genes in the closest proximity (within 100kb) to enhD in the categories depicted in 5B. Bars represent genes that were up- (orange) or down-regulated (blue) by more than 1.5 fold in TKO versus Het, or unchanged (grey). The total number of genes associated with each enhD category is indicated above the histogram. **D.** GO term analysis by enrichR associated with upregulated genes closest to upregulated enhD. **E.** Genome view of stranded chromatin-enriched (green) and cytosolic (red) RNA densities on the *Col6a1 Col6a2* locus, together with ATACseq densities in Het and TKO, showing TKO-specific ATACseq density (brown arrows) colocalizing with TKO-specific RNA (green and red arrows) and a group of enhD elements depicted in the cCRE lane. Yellow bars, enhD/enhP; red bars, Prom; blue bar, CTCF, as annotated in Supp.Fig. 5A. **F, G.** GO term analysis by enrichR associated with upregulated genes upon depletion of the indicated RNA exosome components.

Supplementary Figure 5: A. Number of CTCF ChIPseq peaks located at the cCRE regulatory elements labelled according to the ENCODE cCRE classifications (right panel). Bars represent CTCF peaks that were up- (brown) or down-regulated (blue) by more than 2 fold in TKO versus Het, or changed by less than 20 percent (Unchanged, grey). **B.** Average density profiles on enhD elements. Top panels, ATACseq profiles, and bottom panels, chromatin-associated RNA density profiles in triplicate Het (blue profiles) and TKO (red profiles) samples on enhD elements in the cCRE ENCODE database. EnhD were categorized based on their chromatin accessibility by ATACseq between Het and TKO. Categories are as follows: Down, with decreased accessibility in TKO cells; Unchanged, active in both conditions; Up, with increased accessibility in TKO cells; inactive, with no ATACseq density, respectively. **C.** List of Collagen genes dysregulated in Het versus TKO by DESeq2 analysis. Base mean is their mean expression levels in both Het and TKO, log2FC is the fold change in TKO versus Het, with adjusted p-values. **D.** Average density profiles on LTR retroelements. Top panels, ATACseq profiles, and bottom panels, chromatin-associated RNA density profiles in triplicate Het (blue profiles) and TKO (red profiles) samples. TKO-only LTRs and Het-only LTRs correspond to the categories of extragenic expressed LTRs depicted in Fig. 2B. Random LTR is a subset of 5,700 LTR elements in the Repat Masker database chosen randomly.

Figure 6: HP1 expression affects collagen genes in hepatocellular carcinoma (HCC) patient samples.
A. Table of patient ranking in high HP1 (Hi HP1) and Low HP1 (Lo HP1) expressing samples based on their cumulative total HP1 expression levels, and compared with gene expression of individual HP1 isoforms. Molecular subclasses (MO) sorted by increasing severity of the disease from MO1 to MO4, and patient survival criteria have been analyzed in Candia *et al.*, 2020. **B.** Unsupervised PCA analysis of patient samples. **C.** Quantification of the accumulation of unstable mRNAs in Lo HP1 and Hi HP1 groups using the RNA HiLo ratio analysis as in Mullani *et al.*, 2021. ***, p-value : 9.94E-06 (two-tailed Student's t-test). **D.** Histograms of fold changes in expression of the indicated dysregulated genes in Lo HP1versus Hi HP1 patients. Adjusted p-values: 0.00108, 2.49E-07, 7.09E-07, 5.44E-05, 7.75E-07, 0.0194, 9.96E-08, and 0.00742, from top to bottom, respectively. **E, F.** Histograms of the most significant indicated Gene Ontology (GO) terms and their adjusted p-values for upregulated genes in Lo HP1 patient samples. **G.** Summary of tumor characteristics in the Hi and Lo HP1 groups.

Supplementary Figure 6:
A, Histogram of total HP1 expression ratio in tumors relative to adjacent non-tumor samples of 76 HCC patient transcriptomes (GSE144269, Candia *et al.* 2020). **B.** Kaplan-Meyer plots of liver cancer patient survival probabilities in the Human Protein Atlas database (proteinatlas.org) associated with *CBX1* (HP1β), *CBX3* (HP1γ), and *CBX5* (HP1α). Survival curves for low expression (blue) are compared to high expression (pink) of the indicated genes. P scores indicate log-rank P values of correlation between expression levels and patient survival. **C.** Total HP1 expression levels in the two groups of high HP1 (Hi HP1) and Low HP1 (Lo HP1) patients defined by the first and third total HP1 expression quartiles, respectively. **D, E,** Histograms of the number of Hi HP1 and Lo HP1 patients clustered according to four Molecular subclasses (MO) sorted by increasing severity of the disease from MO1 to MO4 (D), or showing survival criteria (E), as defined in Candia *et al.*, 2020. **F.** Histograms of the most significant KEGG (Kyoto Encyclopedia of Genes and Genomes) pathways corresponding to upregulated genes in Hi HP1, sorted by adjusted p-values.

References

Allo M, Buggiano V, Fededa JP, Petrillo E, Schor I, De La Mata M, Agirre E, Plass M, Eyras E, Elela SA *et al* (2009) Control of alternative splicing through siRNA-mediated transcriptional gene silencing. ***Nat Struct Mol Biol* 16:** 717-24

Ameyar-Zazoua M, Rachez C, Souidi M, Robin P, Fritsch L, Young R, Morozova N, Fenouil R, Descostes N, Andrau JC *et al* (2012) Argonaute proteins couple chromatin silencing to alternative splicing. ***Nat Struct Mol Biol* 19:** 998-1004

Andersen PR, Domanski M, Kristiansen MS, Storvall H, Ntini E, Verheggen C, Schein A, Bunkenborg J, Poser I, Hallais M *et al* (2013) The human cap-binding complex is functionally connected to the nuclear RNA exosome. ***Nat Struct Mol Biol* 20:** 1367-76

Andersson R, Gebhard C, Miguel-Escalada I, Hoof I, Bornholdt J, Boyd M, Chen Y, Zhao X, Schmidl C, Suzuki T *et al* (2014) An atlas of active enhancers across human cell types and tissues. ***Nature* 507:** 455-461

Azebi S, Batsche E, Michel F, Kornobis E, Muchardt C (2019) Expression of endogenous retroviruses reflects increased usage of atypical enhancers in T cells. ***EMBO J* 38**

Bannister AJ, Zegerman P, Partridge JF, Miska EA, Thomas JO, Allshire RC, Kouzarides T (2001) Selective recognition of methylated lysine 9 on histone H3 by the HP1 chromo domain. ***Nature* 410:** 120-4

Bryan LC, Weilandt DR, Bachmann AL, Kilic S, Lechner CC, Odermatt PD, Fantner GE, Georgeon S, Hantschel O, Hatzimanikatis V *et al* (2017) Single-molecule kinetic analysis of HP1-chromatin binding reveals a dynamic network of histone modification and DNA interactions. ***Nucleic Acids Res* 45:** 10504-10517

Buenrostro JD, Giresi PG, Zaba LC, Chang HY, Greenleaf WJ (2013) Transposition of native chromatin for fast and sensitive epigenomic profiling of open chromatin, DNA-binding proteins and nucleosome position. ***Nat Methods* 10:** 1213-8

Buhler M, Haas W, Gygi SP, Moazed D (2007) RNAi-dependent and -independent RNA turnover mechanisms contribute to heterochromatic gene silencing. ***Cell* 129:** 707-21

Bulut-Karslioglu A, De La Rosa-Velazquez IA, Ramirez F, Barenboim M, Onishi-Seebacher M, Arand J, Galan C, Winter GE, Engist B, Gerle B *et al* (2014) Suv39h-dependent H3K9me3 marks intact retrotransposons and silences LINE elements in mouse embryonic stem cells. ***Mol Cell* 55:** 277-90

Calvet S, Sallis S, Saksouk N, Rebouissou C, Teyssier C, Lesne A, Cammas F, Forne T (2022) Endogenous Retroviral Sequences Behave as Putative Enhancers Controlling Gene Expression through HP1-Regulated Long-Range Chromatin Interactions. ***Cells* 11**

Candia J, Bayarsaikhan E, Tandon M, Budhu A, Forgues M, Tovuu LO, Tudev U, Lack J, Chao A, Chinburen J *et al* (2020) The genomic landscape of Mongolian hepatocellular carcinoma. ***Nat Commun* 11:** 4383

Cheutin T, Mcnairn AJ, Jenuwein T, Gilbert DM, Singh PB, Misteli T (2003) Maintenance of stable heterochromatin domains by dynamic HP1 binding. ***Science* 299:** 721-5

Chomczynski P, Sacchi N (2006) The single-step method of RNA isolation by acid guanidinium thiocyanate-phenol-chloroform extraction: twenty-something years on. ***Nat Protoc* 1:** 581-5

Festenstein R, Pagakis SN, Hiragami K, Lyon D, Verreault A, Sekkali B, Kioussis D (2003) Modulation of heterochromatin protein 1 dynamics in primary Mammalian cells. ***Science* 299:** 719-21

Festuccia N, Dubois A, Vandormael-Pournin S, Gallego Tejeda E, Mouren A, Bessonnard S, Mueller F, Proux C, Cohen-Tannoudji M, Navarro P (2016) Mitotic binding of Esrrb marks key regulatory regions of the pluripotency network. ***Nat Cell Biol* 18:** 1139-1148

Fueyo R, Judd J, Feschotte C, Wysocka J (2022) Roles of transposable elements in the regulation of mammalian transcription. ***Nat Rev Mol Cell Biol* 23:** 481-497

Garland W, Muller I, Wu M, Schmid M, Imamura K, Rib L, Sandelin A, Helin K, Jensen TH (2022) Chromatin modifier HUSH co-operates with RNA decay factor NEXT to restrict transposable element expression. ***Mol Cell* 82:** 1691-1707 e8

Grewal SIS (2023) The molecular basis of heterochromatin assembly and epigenetic inheritance. ***Mol Cell* 83:** 1767-1785

Hediger F, Gasser SM (2006) Heterochromatin protein 1: don't judge the book by its cover! ***Curr Opin Genet Dev* 16:** 143-50

Hiragami-Hamada K, Fischle W (2014) RNAs - physical and functional modulators of chromatin reader proteins. ***Biochim Biophys Acta* 1839:** 737-42

Jacobs SA, Taverna SD, Zhang Y, Briggs SD, Li J, Eissenberg JC, Allis CD, Khorasanizadeh S (2001) Specificity of the HP1 chromo domain for the methylated N-terminus of histone H3. ***EMBO J* 20:** 5232-41

Kaya-Okur HS, Wu SJ, Codomo CA, Pledger ES, Bryson TD, Henikoff JG, Ahmad K, Henikoff S (2019) CUT&Tag for efficient epigenomic profiling of small samples and single cells. ***Nat Commun* 10:** 1930

Keller C, Adaixo R, Stunnenberg R, Woolcock KJ, Hiller S, Buhler M (2012) HP1(Swi6) mediates the recognition and destruction of heterochromatic RNA transcripts. ***Mol Cell* 47:** 215-27

Kilchert C, Wittmann S, Vasiljeva L (2016) The regulation and functions of the nuclear RNA exosome complex. ***Nat Rev Mol Cell Biol* 17:** 227-39

Lacava J, Houseley J, Saveanu C, Petfalski E, Thompson E, Jacquier A, Tollervey D (2005) RNA degradation by the exosome is promoted by a nuclear polyadenylation complex. ***Cell* 121:** 713-24

Lachner M, O'carroll D, Rea S, Mechtler K, Jenuwein T (2001) Methylation of histone H3 lysine 9 creates a binding site for HP1 proteins. ***Nature* 410:** 116-20

Laffleur B, Lim J, Zhang W, Chen Y, Pefanis E, Bizarro J, Batista CR, Wu L, Economides AN, Wang J *et al* (2021) Noncoding RNA processing by DIS3 regulates chromosomal architecture and somatic hypermutation in B cells. ***Nat Genet* 53:** 230-242

Lechner MS, Schultz DC, Negorev D, Maul GG, Rauscher FJ, 3rd (2005) The mammalian heterochromatin protein 1 binds diverse nuclear proteins through a common motif that targets the chromoshadow domain. ***Biochem Biophys Res Commun* 331:** 929-37

Lubas M, Andersen PR, Schein A, Dziembowski A, Kudla G, Jensen TH (2015) The human nuclear exosome targeting complex is loaded onto newly synthesized RNA to direct early ribonucleolysis. ***Cell Rep* 10:** 178-92

Lubas M, Christensen MS, Kristiansen MS, Domanski M, Falkenby LG, Lykke-Andersen S, Andersen JS, Dziembowski A, Jensen TH (2011) Interaction profiling identifies the human nuclear exosome targeting complex. ***Mol Cell* 43:** 624-37

Maison C, Bailly D, Peters AH, Quivy JP, Roche D, Taddei A, Lachner M, Jenuwein T, Almouzni G (2002) Higher-order structure in pericentric heterochromatin involves a distinct pattern of histone modification and an RNA component. ***Nat Genet* 30:** 329-34

Maison C, Bailly D, Roche D, Montes De Oca R, Probst AV, Vassias I, Dingli F, Lombard B, Loew D, Quivy JP *et al* (2011) SUMOylation promotes de novo targeting of HP1alpha to pericentric heterochromatin. ***Nat Genet* 43:** 220-7

Mata-Garrido J, Xiang Y, Chang-Marchand Y, Reisacher C, Ageron E, Guerrera IC, Casafont I, Bruneau A, Cherbuy C, Treton X *et al* (2022) The Heterochromatin protein 1 is a regulator in RNA splicing precision deficient in ulcerative colitis. ***Nat Commun* 13:** 6834

Matkovic R, Morel M, Lanciano S, Larrous P, Martin B, Bejjani F, Vauthier V, Hansen MMK, Emiliani S, Cristofari G *et al* (2022) TASOR epigenetic repressor cooperates with a CNOT1 RNA degradation pathway to repress HIV. ***Nat Commun* 13:** 66

Meng ZY, Fan YC, Zhang CS, Zhang LL, Wu T, Nong MY, Wang T, Chen C, Jiang LH (2023) EXOSC10 is a novel hepatocellular carcinoma prognostic biomarker: a comprehensive bioinformatics analysis and experiment verification. ***PeerJ* 11:** e15860

Meola N, Domanski M, Karadoulama E, Chen Y, Gentil C, Pultz D, Vitting-Seerup K, Lykke-Andersen S, Andersen JS, Sandelin A *et al* (2016) Identification of a Nuclear Exosome Decay Pathway for Processed Transcripts. ***Mol Cell* 64:** 520-533

Minc E, Courvalin JC, Buendia B (2000) HP1gamma associates with euchromatin and heterochromatin in mammalian nuclei and chromosomes. ***Cytogenet Cell Genet* 90:** 279-84

Motamedi MR, Hong EJ, Li X, Gerber S, Denison C, Gygi S, Moazed D (2008) HP1 proteins form distinct complexes and mediate heterochromatic gene silencing by nonoverlapping mechanisms. ***Mol Cell* 32:** 778-90

Muchardt C, Guilleme M, Seeler JS, Trouche D, Dejean A, Yaniv M (2002) Coordinated methyl and RNA binding is required for heterochromatin localization of mammalian HP1alpha. ***EMBO Rep* 3:** 975-81

Mullani N, Porozhan Y, Mangelinck A, Rachez C, Costallat M, Batsche E, Goodhardt M, Cenci G, Mann C, Muchardt C (2021) Reduced RNA turnover as a driver of cellular senescence. ***Life Sci Alliance* 4**

Ostapcuk V, Mohn F, Carl SH, Basters A, Hess D, Iesmantavicius V, Lampersberger L, Flemr M, Pandey A, Thoma NH *et al* (2018) Activity-dependent neuroprotective protein recruits HP1 and CHD4 to control lineage-specifying genes. ***Nature* 557:** 739-743

Pefanis E, Wang J, Rothschild G, Lim J, Kazadi D, Sun J, Federation A, Chao J, Elliott O, Liu ZP *et al* (2015) RNA exosome-regulated long non-coding RNA transcription controls super-enhancer activity. ***Cell* 161:** 774-89

Phillips JE, Corces VG (2009) CTCF: master weaver of the genome. ***Cell* 137:** 1194-211

Piacentini L, Fanti L, Negri R, Del Vescovo V, Fatica A, Altieri F, Pimpinelli S (2009) Heterochromatin protein 1 (HP1a) positively regulates euchromatic gene expression through RNA transcript association and interaction with hnRNPs in Drosophila. ***PLoS Genet* 5:** e1000670

Porozhan Y, Carstensen M, Thouroude S, Costallat M, Rachez C, Batsche E, Petersen T, Christensen T, Muchardt C (2024) Defective Integrator activity shapes the transcriptome of patients with multiple sclerosis. ***Life Sci Alliance* 7**

Preker P, Nielsen J, Kammler S, Lykke-Andersen S, Christensen MS, Mapendano CK, Schierup MH, Jensen TH (2008) RNA exosome depletion reveals transcription upstream of active human promoters. ***Science* 322:** 1851-4

Rachez C, Legendre R, Costallat M, Varet H, Yi J, Kornobis E, Muchardt C (2021) HP1gamma binding pre-mRNA intronic repeats modulates RNA splicing decisions. ***EMBO Rep* 22:** e52320

Rambout X, Maquat LE (2024) Nuclear mRNA decay: regulatory networks that control gene expression. ***Nat Rev Genet* 25:** 679-697

Saint-Andre V, Batsche E, Rachez C, Muchardt C (2011) Histone H3 lysine 9 trimethylation and HP1gamma favor inclusion of alternative exons. ***Nat Struct Mol Biol* 18:** 337-44

Saksouk N, Hajdari S, Perez Y, Pratlong M, Barrachina C, Graber C, Gregoire D, Zavoriti A, Sarrazin A, Pirot N *et al* (2020) The mouse HP1 proteins are essential for preventing liver tumorigenesis. ***Oncogene* 39:** 2676-2691

Sartorelli V, Lauberth SM (2020) Enhancer RNAs are an important regulatory layer of the epigenome. ***Nat Struct Mol Biol* 27:** 521-528

Schaukowitch K, Joo JY, Liu X, Watts JK, Martinez C, Kim TK (2014) Enhancer RNA facilitates NELF release from immediate early genes. ***Mol Cell* 56:** 29-42

Silla T, Schmid M, Dou Y, Garland W, Milek M, Imami K, Johnsen D, Polak P, Andersen JS, Selbach M *et al* (2020) The human ZC3H3 and RBM26/27 proteins are critical for PAXT-mediated nuclear RNA decay. ***Nucleic Acids Res* 48:** 2518-2530

Skourti-Stathaki K, Kamieniarz-Gdula K, Proudfoot NJ (2014) R-loops induce repressive chromatin marks over mammalian gene terminators. ***Nature* 516:** 436-9

Smallwood A, Hon GC, Jin F, Henry RE, Espinosa JM, Ren B (2012) CBX3 regulates efficient RNA processing genome-wide. ***Genome Res* 22:** 1426-36

Thiru A, Nietlispach D, Mott HR, Okuwaki M, Lyon D, Nielsen PR, Hirshberg M, Verreault A, Murzina NV, Laue ED (2004) Structural basis of HP1/PXVXL motif peptide interactions and HP1 localisation to heterochromatin. ***EMBO J* 23:** 489-99

Tomecki R, Drazkowska K, Kobylecki K, Tudek A (2023) SKI complex: A multifaceted cytoplasmic RNA exosome cofactor in mRNA metabolism with links to disease, developmental processes, and antiviral responses. ***Wiley Interdiscip Rev RNA* 14:** e1795

Vakoc CR, Mandat SA, Olenchock BA, Blobel GA (2005) Histone H3 lysine 9 methylation and HP1gamma are associated with transcription elongation through mammalian chromatin. ***Mol Cell* 19:** 381-91

Weick EM, Lima CD (2021) RNA helicases are hubs that orchestrate exosome-dependent 3'-5' decay. ***Curr Opin Struct Biol* 67:** 86-94

Winczura K, Schmid M, Iasillo C, Molloy KR, Harder LM, Andersen JS, Lacava J, Jensen TH (2018) Characterizing ZC3H18, a Multi-domain Protein at the Interface of RNA Production and Destruction Decisions. ***Cell Rep* 22:** 44-58

Wu Y, Liu W, Chen J, Liu S, Wang M, Yang L, Chen C, Qi M, Xu Y, Qiao Z *et al* (2019) Nuclear Exosome Targeting Complex Core Factor Zcchc8 Regulates the Degradation of LINE1 RNA in Early Embryos and Embryonic Stem Cells. ***Cell Rep* 29:** 2461-2472 e6

Yearim A, Gelfman S, Shayevitch R, Melcer S, Glaich O, Mallm JP, Nissim-Rafinia M, Cohen AH, Rippe K, Meshorer E *et al* (2015) HP1 is involved in regulating the global impact of DNA methylation on alternative splicing. ***Cell Rep* 10:** 1122-34

Zaidan NZ, Walker KJ, Brown JE, Schaffer LV, Scalf M, Shortreed MR, Iyer G, Smith LM, Sridharan R (2018) Compartmentalization of HP1 Proteins in Pluripotency Acquisition and Maintenance. ***Stem Cell Reports*** **10:** 627-641

Zhang Y, Stefanovic B (2016) LARP6 Meets Collagen mRNA: Specific Regulation of Type I Collagen Expression. ***Int J Mol Sci*** **17:** 419

Zhao S, Lu J, Pan B, Fan H, Byrum SD, Xu C, Kim A, Guo Y, Kanchi KL, Gong W *et al* (2023) TNRC18 engages H3K9me3 to mediate silencing of endogenous retrotransposons. ***Nature*** **623:** 633-642

Fig. 1

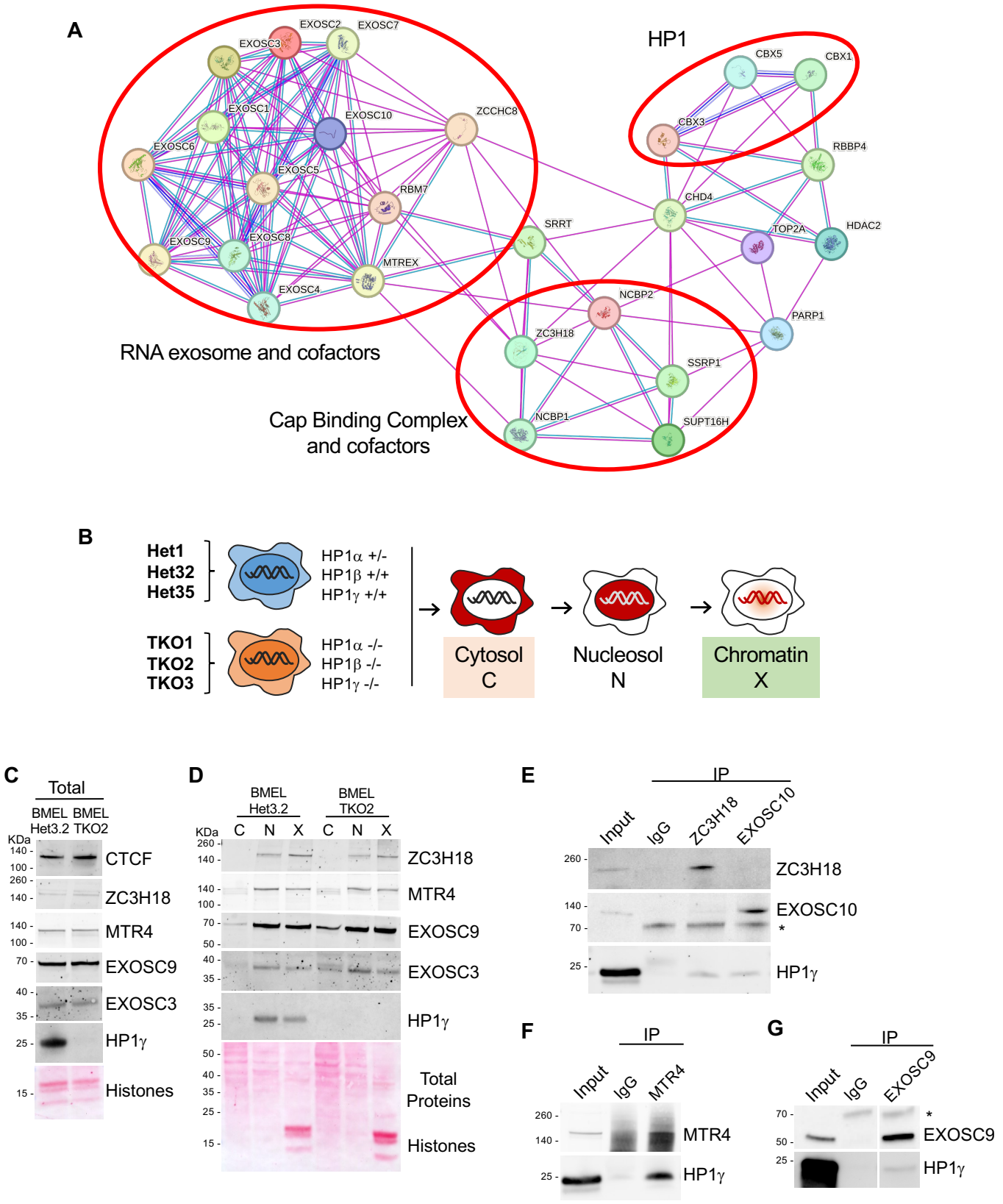
A
EXOSC2
EXOSC7
EXOSC3
EXOSC1
EXOSC10
ZCCHC8
EXOSC6
EXOSC5
RBM7
EXOSC9
EXOSC8
MTREX
EXOSC4
RNA exosome and cofactors
HP1
CBX5
CBX1
CBX3
RBBP4
CHD4
SRRT
TOP2A
HDAC2
NCBP2
PARP1
ZC3H18
SSRP1
NCBP1
SUPT16H
Cap Binding Complex
and cofactors
B
Het1
Het32
Het35
HP1α +/-
HP1β +/+
HP1γ +/+
TKO1
TKO2
TKO3
HP1α -/-
HP1β -/-
HP1γ -/-
Cytosol
C
Nucleosol
N
Chromatin
X
C
Total
BMEL Het3.2
BMEL TKO2
KDa
CTCF
ZC3H18
MTR4
EXOSC9
EXOSC3
HP1γ
Histones
D
BMEL Het3.2
BMEL TKO2
C N X C N X
KDa
ZC3H18
MTR4
EXOSC9
EXOSC3
HP1γ
Total Proteins
Histones
E
IP
Input
IgG
ZC3H18
EXOSC10
ZC3H18
EXOSC10
*
HP1γ
F
IP
Input
IgG
MTR4
MTR4
HP1γ
G
IP
Input
IgG
EXOSC9
*
EXOSC9
HP1γ

Supplementary Fig. 1

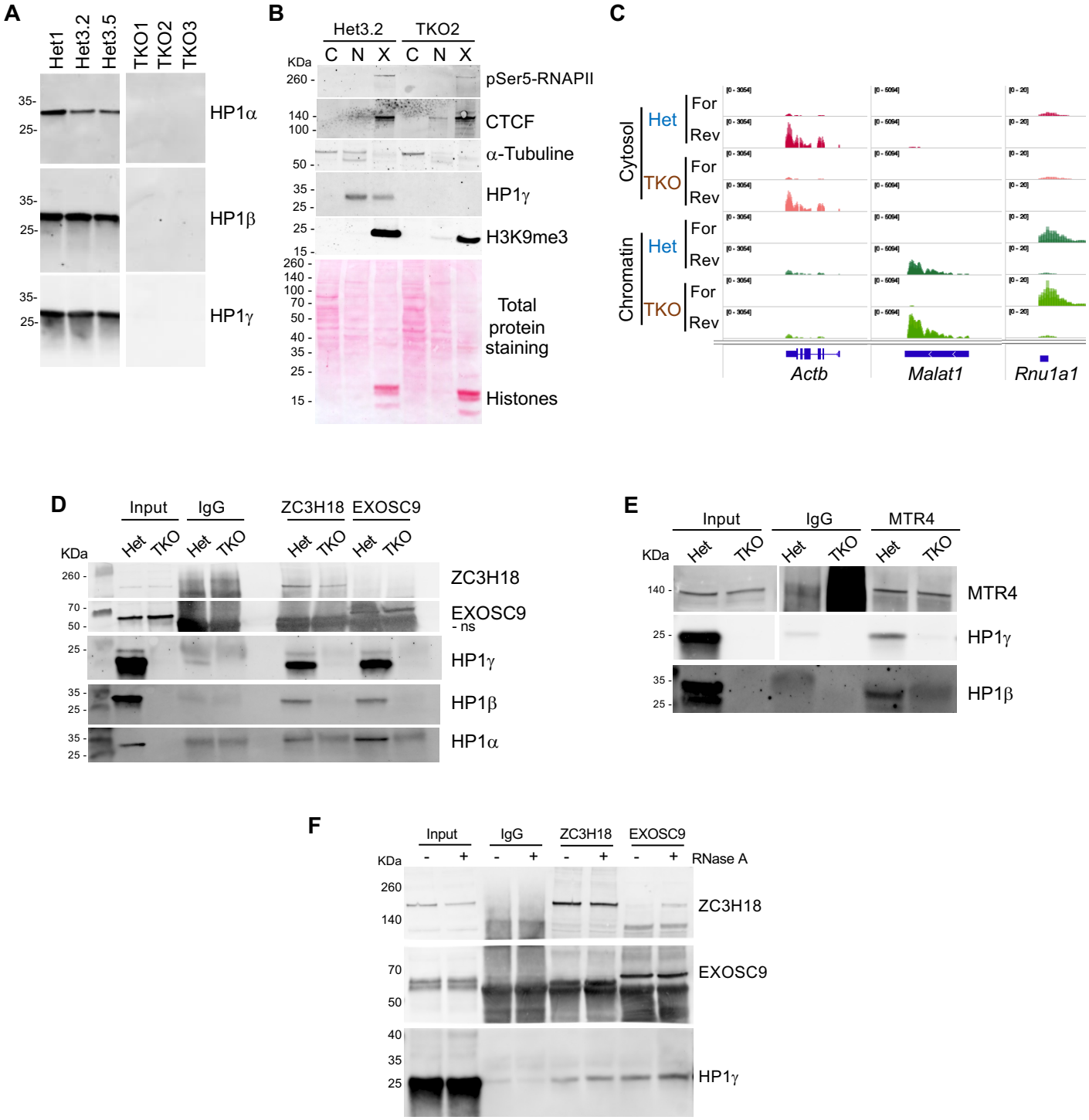

Fig. 2

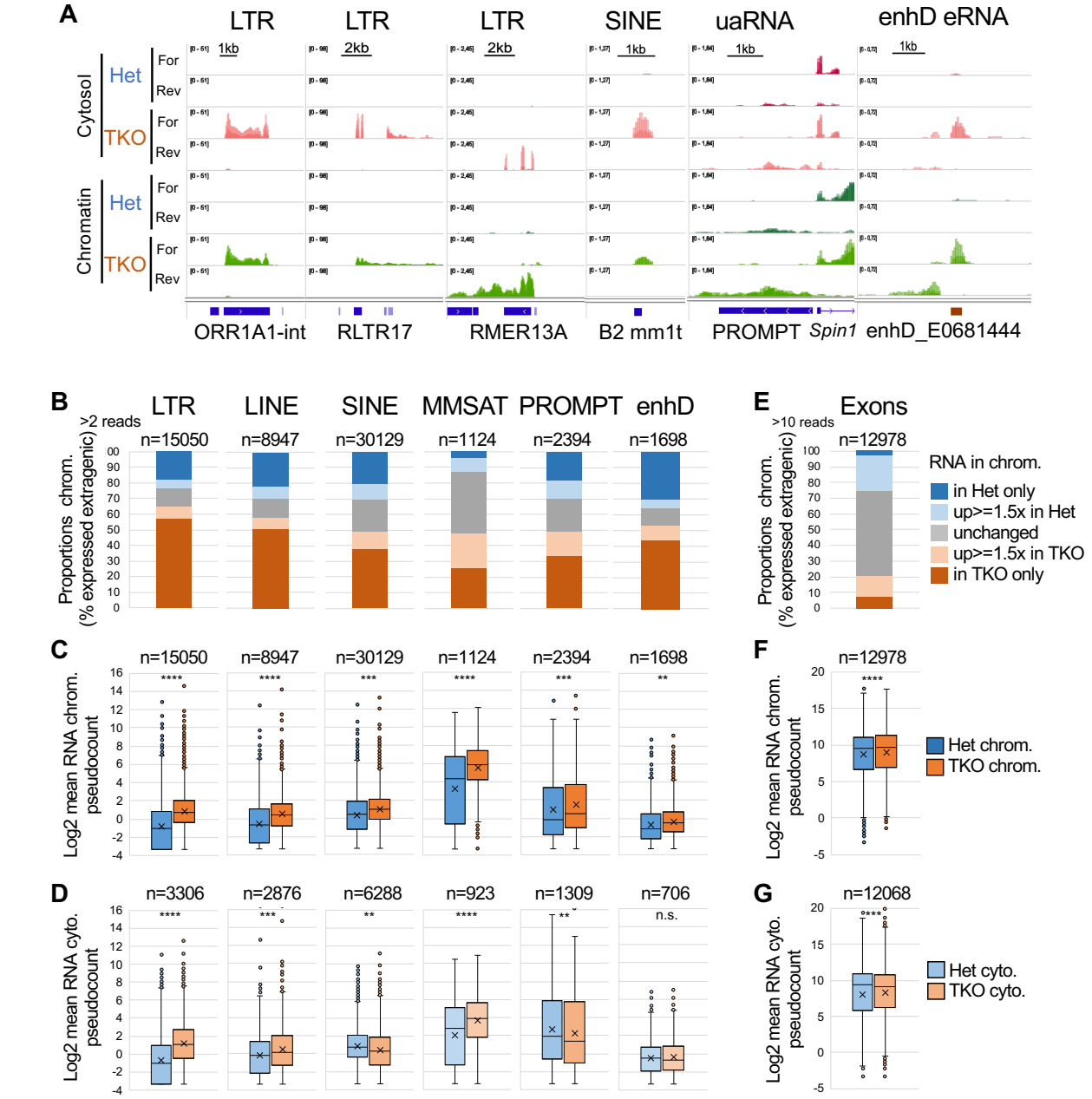
A
LTR
LTR
LTR
SINE
uaRNA
enhD eRNA
Cytosol
Chromatin
Het
TKO
For
Rev
1kb
2kb
ORR1A1-int
RLTR17
RMER13A
B2 mm1t
PROMPT
Spin1
enhD_E0681444
B
LTR
LINE
SINE
MMSAT
PROMPT
enhD
>2 reads
n=15050
n=8947
n=30129
n=1124
n=2394
n=1698
Proportions chrom. (% expressed extragenic)
E
Exons
>10 reads
n=12978
RNA in chrom.
in Het only
up>=1.5x in Het
unchanged
up>=1.5x in TKO
in TKO only
C
Log2 mean RNA chrom. pseudocount
F
Het chrom.
TKO chrom.
D
n=3306
n=2876
n=6288
n=923
n=1309
n=706
n.s.
Log2 mean RNA cyto. pseudocount
G
n=12068
Het cyto.
TKO cyto.
H
chr8:124,085,599-124,097,851
chr1:50,806,631-50,828,650
chr2:45,689,912-45,714,333
chr2:162,382,528-162,410,093
Cyto. RNA
Chrom. RNA
Garland et al. 2022
ESC control
Zfc3h1 KO
Zcchc8 KO
LTR

Fig. 3

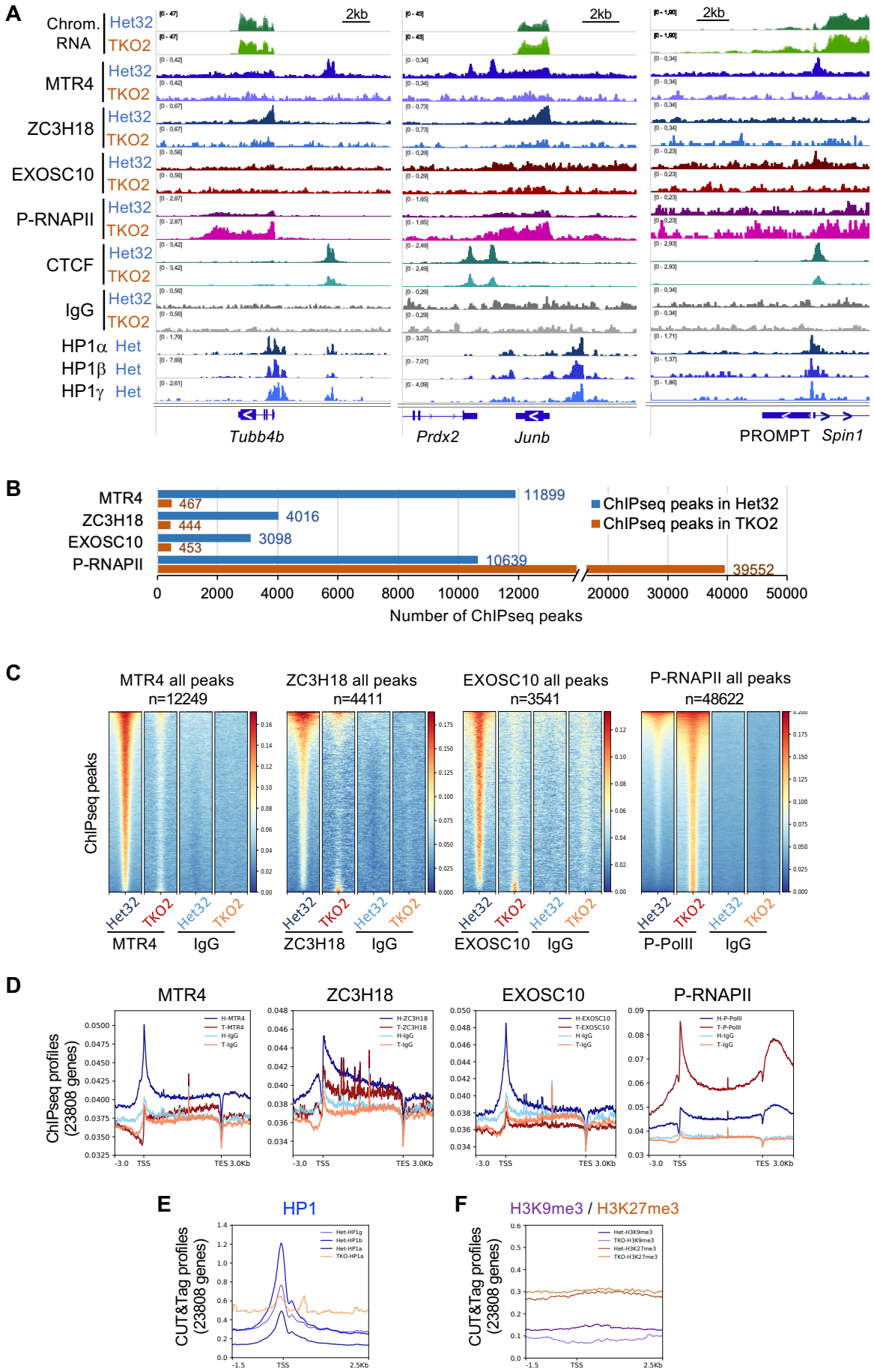
A
Chrom. RNA
Het32
TKO2
MTR4
ZC3H18
EXOSC10
P-RNAPII
CTCF
IgG
HP1α Het
HP1β Het
HP1γ Het
2kb
Tubb4b
Prdx2
Junb
PROMPT
Spin1
B
MTR4
ZC3H18
EXOSC10
P-RNAPII
467
11899
444
4016
453
3098
10639
39552
ChIPseq peaks in Het32
ChIPseq peaks in TKO2
Number of ChIPseq peaks
C
MTR4 all peaks
n=12249
ZC3H18 all peaks
n=4411
EXOSC10 all peaks
n=3541
P-RNAPII all peaks
n=48622
ChIPseq peaks
Het32
TKO2
MTR4
IgG
ZC3H18
EXOSC10
P-PolII
D
MTR4
ZC3H18
EXOSC10
P-RNAPII
ChIPseq profiles (23808 genes)
TSS
TES 3.0Kb
E
HP1
CUT&Tag profiles (23808 genes)
TSS
2.5Kb
F
H3K9me3 / H3K27me3
CUT&Tag profiles (23808 genes)
TSS
2.5Kb

Supplementary Fig. 3

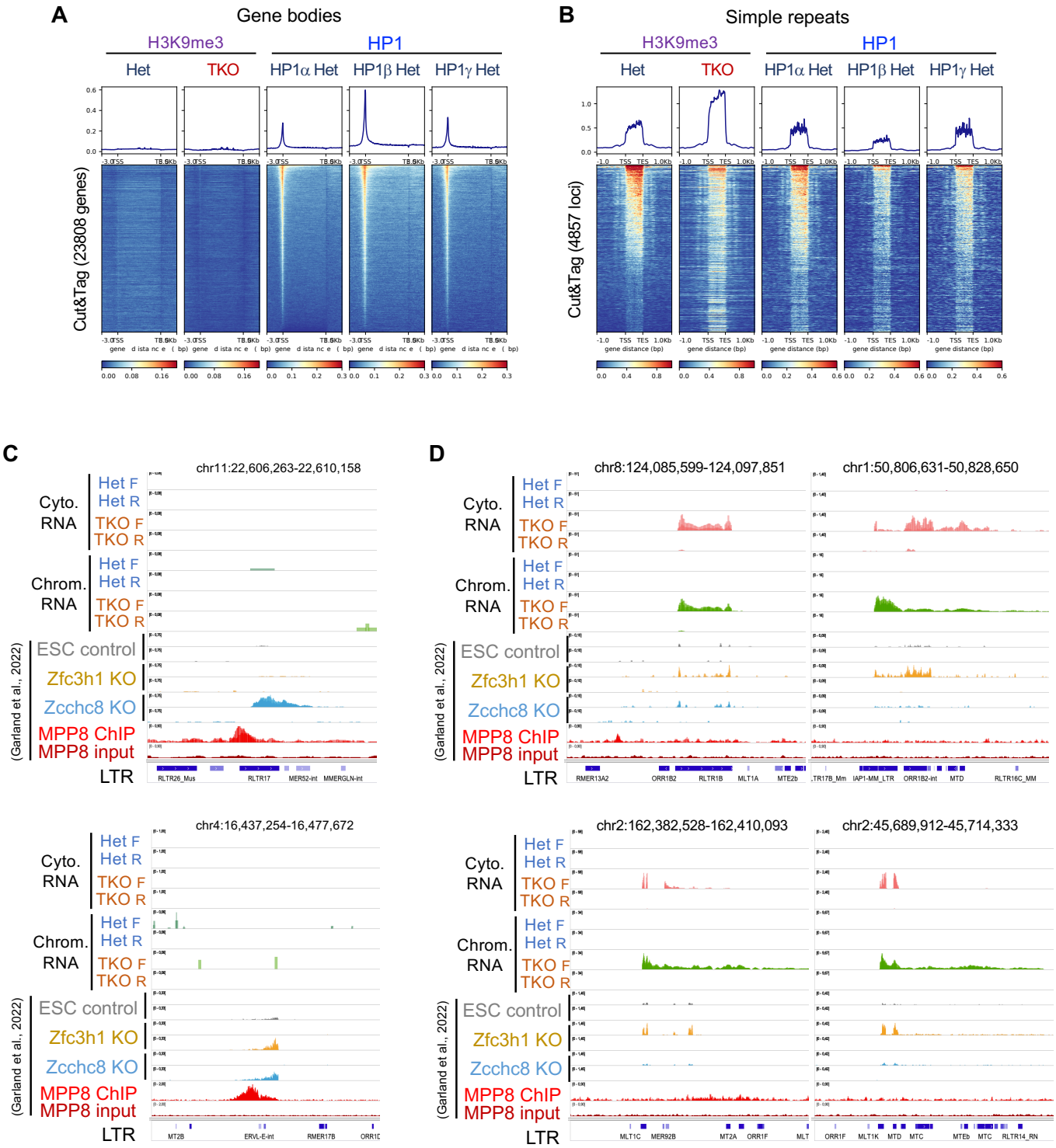

Fig. 4

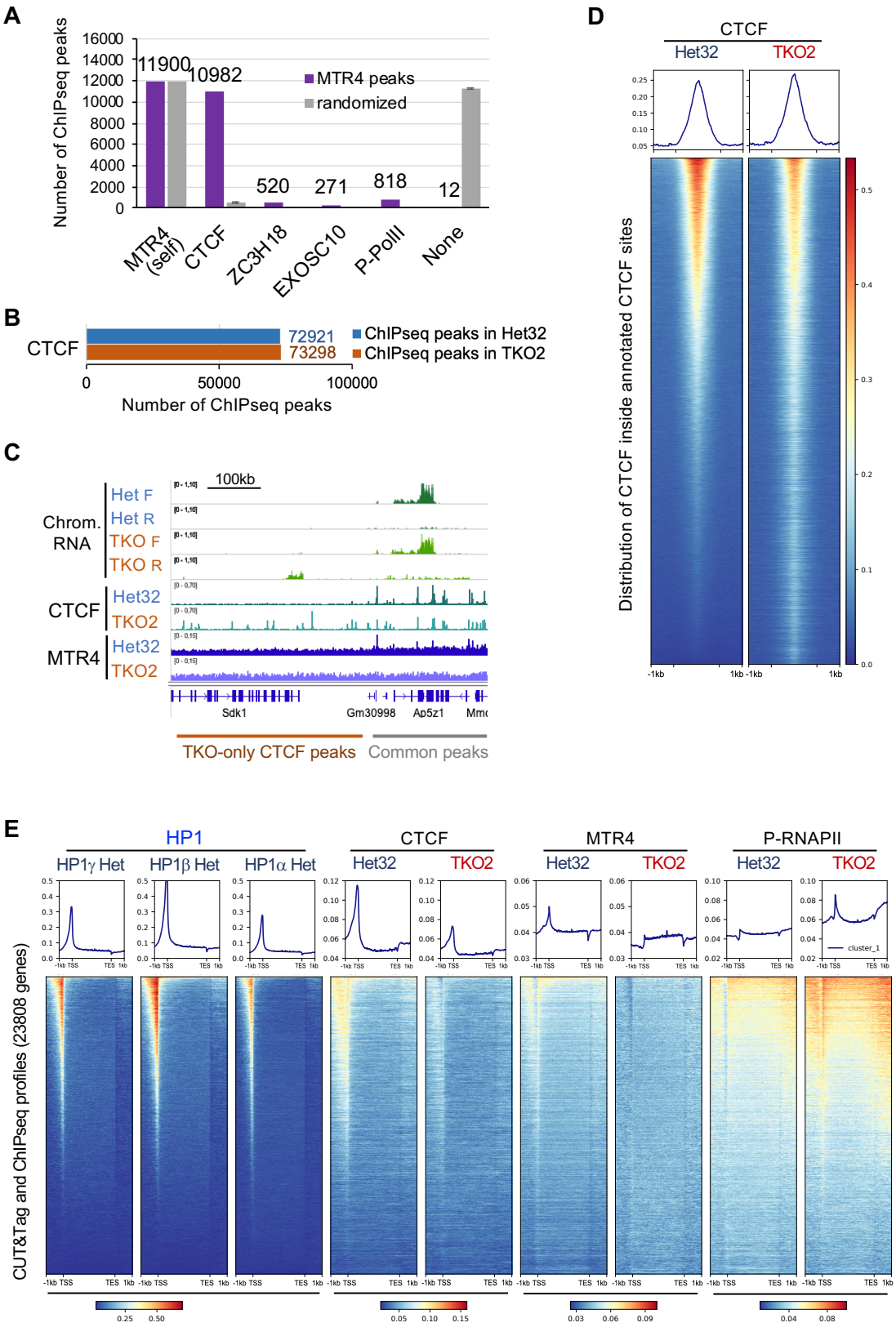
A
Number of ChIPseq peaks
16000
14000
12000
10000
8000
6000
4000
2000
0
11900
10982
520
271
818
12
MTR4 peaks
randomized
MTR4 (self)
CTCF
ZC3H18
EXOSC10
P-PolII
None
B
CTCF
72921
73298
ChIPseq peaks in Het32
ChIPseq peaks in TKO2
0
50000
100000
Number of ChIPseq peaks
C
100kb
Chrom. RNA
Het F
Het R
TKO F
TKO R
CTCF
Het32
TKO2
MTR4
Het32
TKO2
Sdk1
Gm30998
Ap5z1
TKO-only CTCF peaks
Common peaks
D
CTCF
Het32
TKO2
Distribution of CTCF inside annotated CTCF sites
-1kb
1kb
E
HP1
HP1γ Het
HP1β Het
HP1α Het
CTCF
Het32
TKO2
MTR4
Het32
TKO2
P-RNAPII
Het32
TKO2
CUT&Tag and ChIPseq profiles (23808 genes)
-1kb TSS
TES 1kb

Fig. 5

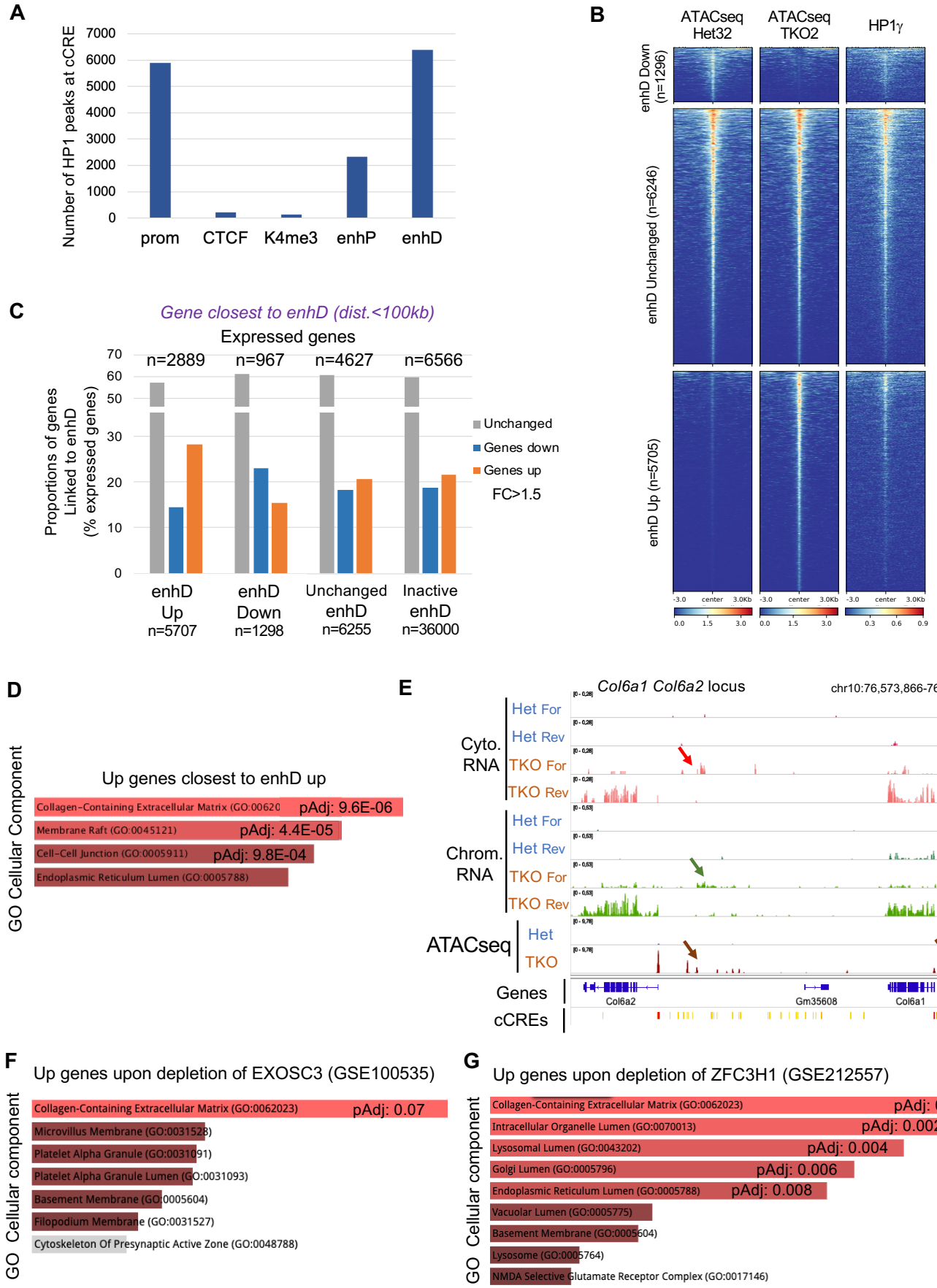
A
Number of HP1 peaks at cCRE
7000
6000
5000
4000
3000
2000
1000
0
prom
CTCF
K4me3
enhP
enhD
B
ATACseq Het32
ATACseq TKO2
HP1γ
enhD Down (n=1296)
enhD Unchanged (n=6246)
enhD Up (n=5705)
-3.0
center
3.0Kb
C
Gene closest to enhD (dist.<100kb)
Expressed genes
Proportions of genes Linked to enhD (% expressed genes)
n=2889
n=967
n=4627
n=6566
Unchanged
Genes down
Genes up
FC>1.5
enhD Up n=5707
enhD Down n=1298
Unchanged enhD n=6255
Inactive enhD n=36000
D
GO Cellular Component
Up genes closest to enhD up
Collagen-Containing Extracellular Matrix (GO:00620
pAdj: 9.6E-06
Membrane Raft (GO:0045121)
pAdj: 4.4E-05
Cell-Cell Junction (GO:0005911)
pAdj: 9.8E-04
Endoplasmic Reticulum Lumen (GO:0005788)
E
Col6a1 Col6a2 locus
chr10:76,573,866-76,841,436
Cyto. RNA
Chrom. RNA
ATACseq
Het For
Het Rev
TKO For
TKO Rev
Het
TKO
Genes
cCREs
Col6a2
Gm35608
Col6a1
F
Up genes upon depletion of EXOSC3 (GSE100535)
GO Cellular component
Collagen-Containing Extracellular Matrix (GO:0062023)
pAdj: 0.07
Microvillus Membrane (GO:0031528)
Platelet Alpha Granule (GO:0031091)
Platelet Alpha Granule Lumen (GO:0031093)
Basement Membrane (GO:0005604)
Filopodium Membrane (GO:0031527)
Cytoskeleton Of Presynaptic Active Zone (GO:0048788)
G
Up genes upon depletion of ZFC3H1 (GSE212557)
GO Cellular component
Collagen-Containing Extracellular Matrix (GO:0062023)
pAdj: 0.002
Intracellular Organelle Lumen (GO:0070013)
pAdj: 0.002
Lysosomal Lumen (GO:0043202)
pAdj: 0.004
Golgi Lumen (GO:0005796)
pAdj: 0.006
Endoplasmic Reticulum Lumen (GO:0005788)
pAdj: 0.008
Vacuolar Lumen (GO:0005775)
Basement Membrane (GO:0005604)
Lysosome (GO:0005764)
NMDA Selective Glutamate Receptor Complex (GO:0017146)

Supplementary Fig. 5

A

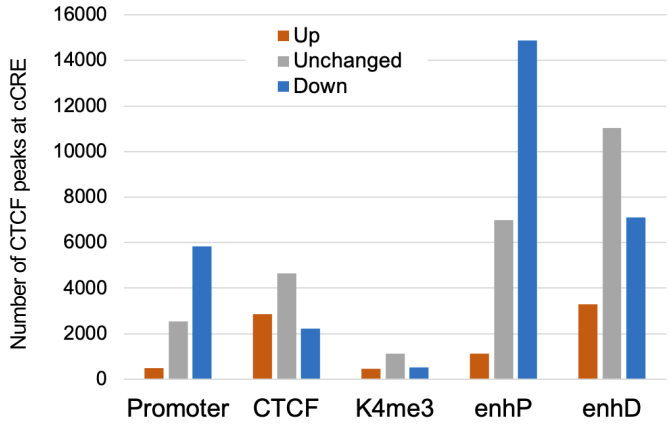

Labels	ENCODE classifications
Prom	promoter-like signature
CTCF	CTCF-only
K4me3	DNase-H3K4me3
enhP	proximal enhancer-like signature
enhD	distal enhancer-like signature

B

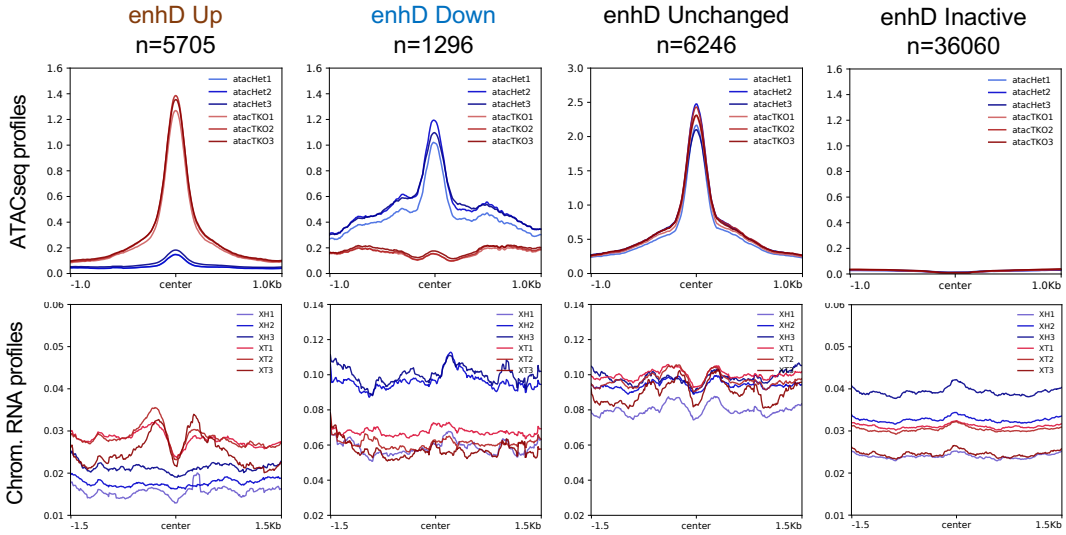

C

Collagen Transcriptome (DESeq2)

Gene name	BaseMean	log2FC	adj-pVal	
Col1a1	26	2.25	4.98E-02	*
Col2a1	62	5.86	2.54E-05	***
Col4a1	4191	0.31	9.29E-01	
Col4a2	2231	0.16	9.67E-01	
Col4a4	34	1.28	7.31E-01	
Col4a5	1575	-0.80	8.08E-01	
Col5a1	939	0.77	9.10E-01	
Col6a1	38	3.94	1.02E-02	*
Col6a2	45	7.51	9.37E-05	****
Col6a3	43	4.22	1.91E-06	****
Col7a1	153	1.62	7.91E-02	
Col9a3	112	0.42	8.16E-01	
Col11a2	311	-0.06	9.92E-01	
Col12a1	91	-1.61	3.88E-01	
Col15a1	144	-1.22	3.15E-01	
Col16a1	57	4.01	2.66E-04	****
Col17a1	14	1.34	6.46E-01	
Col18a1	2373	0.38	7.94E-01	
Col20a1	300	0.68	8.62E-01	
Col24a1	36	0.62	8.92E-01	
Col27a1	198	2.28	3.91E-02	*

D

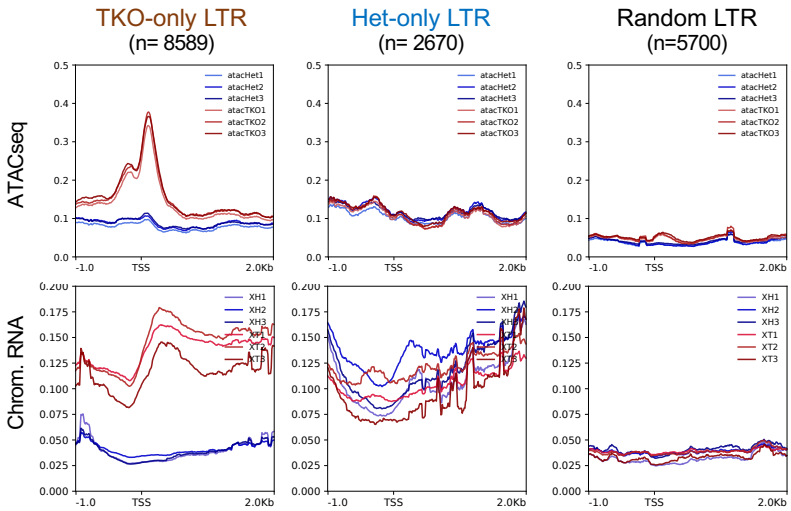

Fig. 6

A

Group	Patient	CBX1	CBX3	CBX5	Total HP1	MO	Survival
Hi HP1	11	26.58	51.31	20.11	98	MO4	Deceased
Hi HP1	13	15.16	38.15	26.88	80.19	MO3	Deceased
Hi HP1	18	31.07	35.9	6.253	73.223	MO2	Deceased
Hi HP1	1	11.98	52.04	3.303	67.323	MO4	Deceased
Hi HP1	20	23.36	52.33	21.89	97.58	MO4	Deceased
Hi HP1	21	59.8	33	30.24	123.04	MO4	Deceased
Hi HP1	30	43.82	59.86	41.78	145.46	MO1	Deceased
Hi HP1	3	31.47	43.53	8.316	83.316	MO4	Deceased
Hi HP1	40	17.39	56.2	9.783	83.373	MO3	Alive
Hi HP1	51	26.22	34.83	13.47	74.52	MO1	Alive
Hi HP1	53	19.59	63.39	22.81	105.79		Deceased
Hi HP1	55	9.006	39.34	16.46	64.806	MO1	Alive
Hi HP1	61	65.77	70.46	57.78	194.01	MO4	Alive
Hi HP1	63	33.45	47.16	4.397	85.007		
Hi HP1	65	11.07	60.54	15.2	86.81	MO4	Alive
Hi HP1	66	21.23	57.28	13.82	92.33	MO1	Alive
Hi HP1	67	28.14	45.95	31.22	105.31	MO3	Deceased
Hi HP1	9	25.42	28.98	8.282	62.682	MO4	Alive
Lo HP1	12	5.745	11.64	6.431	23.816	MO2	Alive
Lo HP1	17	2.253	4.912	2.557	9.722	MO1	Alive
Lo HP1	26	3.459	9.933	5.034	18.426	MO1	Alive
Lo HP1	28	3.673	5.533	4.079	13.285	MO2	Alive
Lo HP1	29	2.874	9.668	4.793	17.335	MO3	Deceased
Lo HP1	2	5.678	13.82	6.402	25.9	MO3	Alive
Lo HP1	32	2.295	7.094	1.152	10.541	MO3	Deceased
Lo HP1	34	3.079	11.32	3.245	17.644	MO1	Alive
Lo HP1	35	3.109	7.974	3.899	14.982	MO2	Alive
Lo HP1	36	6.416	11.13	7.147	24.693	MO2	Alive
Lo HP1	44	3.712	10.44	3.583	17.735	MO4	Alive
Lo HP1	45	3.535	13.14	2.123	18.798	MO1	Alive
Lo HP1	46	0.9888	2.456	0.8371	4.2819	MO2	Alive
Lo HP1	47	1.051	8.005	1.257	10.313		Deceased
Lo HP1	52	7.036	11.39	2.564	20.99	MO4	Alive
Lo HP1	56	1.514	5.67	1.838	9.022	MO1	Alive
Lo HP1	58	1.272	3.102	1.945	6.319	MO3	Alive
Lo HP1	59	0.7354	7.267	0.188	8.1904	MO1	Deceased

B

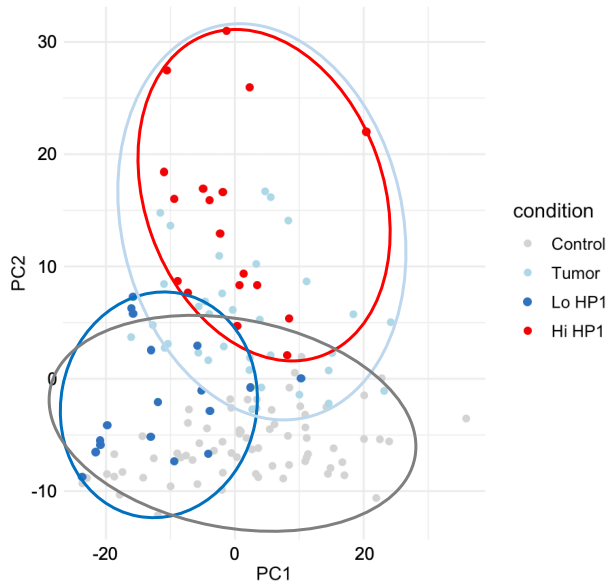

C

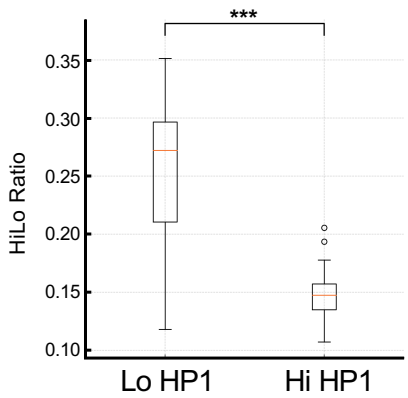

D

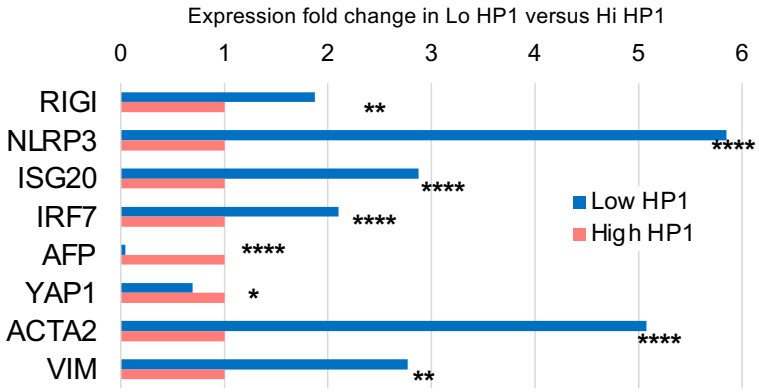

E

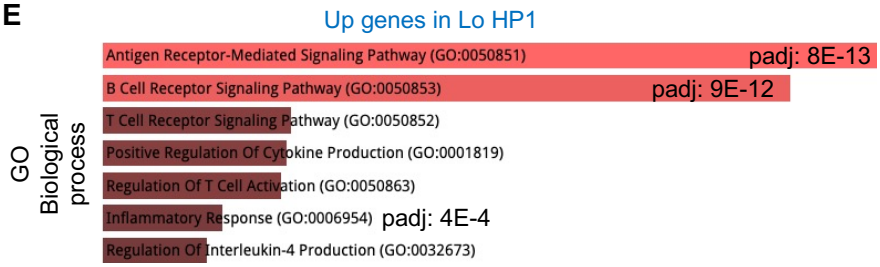

F

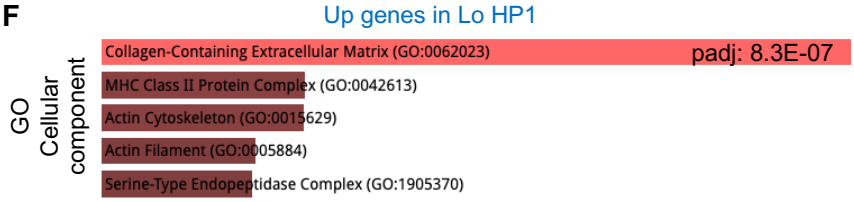

G

	Hi HP1 tumors	Lo HP1 tumors
HP1expression	High	Low
Proliferation	High	Low
Immune infiltration	Low	High
Mortality	High	Lower
Fibrosis	Low	High
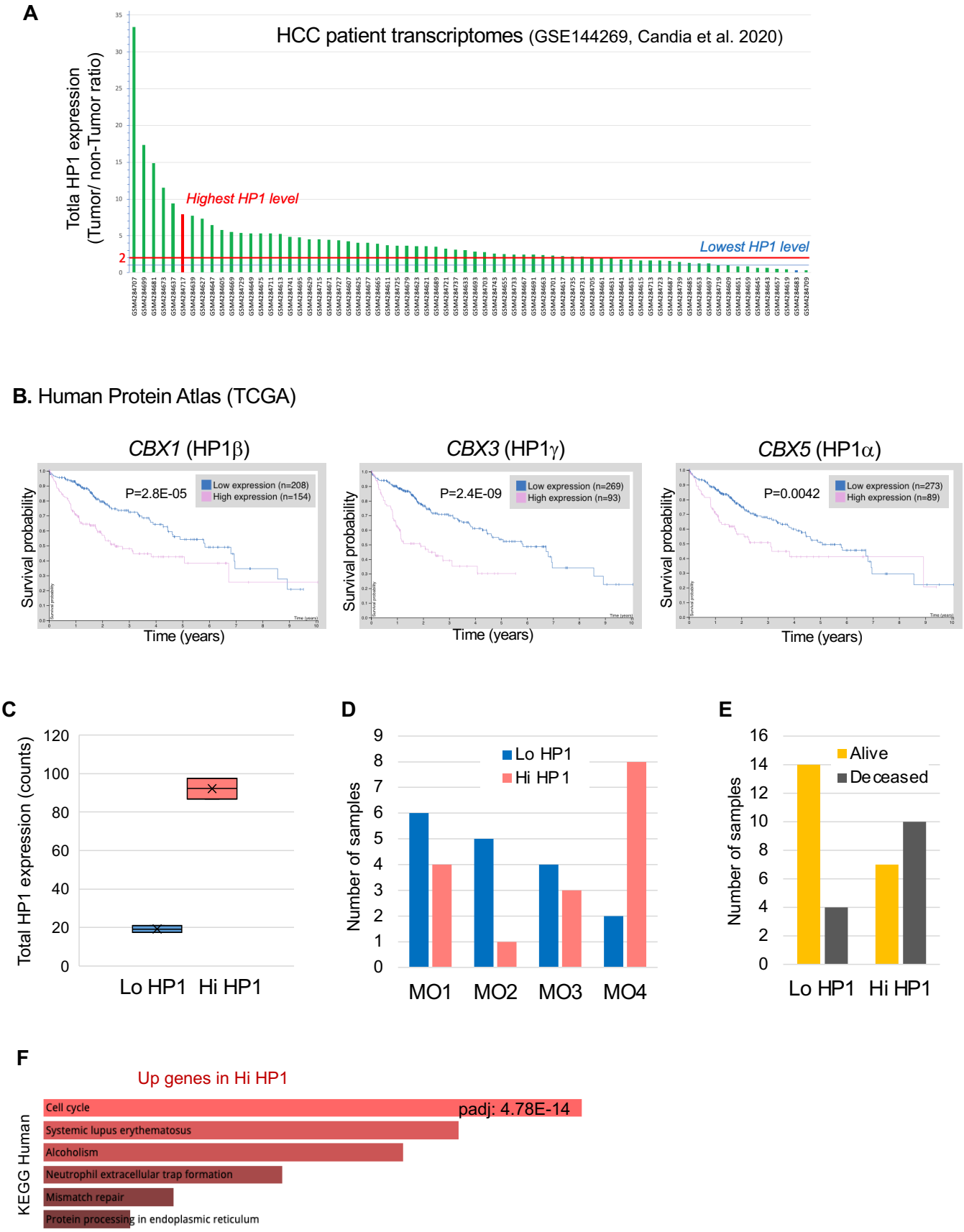
Supplementary Fig. 6